

# 1 Relevance of acoustic methods to quantify bedload transport 2 and bedform dynamics in a large sandy-gravel bed river

3 Jules Le Guern<sup>1</sup>, Stéphane Rodrigues<sup>1,2</sup>, Thomas Geay<sup>3</sup>, Sébastien Zanker<sup>4</sup>, Alexandre Hauet<sup>4</sup>,  
4 Pablo Tassi<sup>5,6</sup>, Nicolas Claude<sup>5,8</sup>, Philippe Jugé<sup>7</sup>, Antoine Duperray<sup>1</sup>, Louis Vervynck<sup>1</sup>.

5 <sup>1</sup>UMR CNRS CITERES, University of Tours, France.

6 <sup>2</sup>Graduate School of Engineering Polytech Tours, University of Tours, France.

7 <sup>3</sup>BURGEAP R&D, Grenoble, France.

8 <sup>4</sup>EDF, Division Technique Générale, Grenoble, France.

9 <sup>5</sup>EDF R&D – National Laboratory for Hydraulics and Environment (LNHE), Chatou, France.

10 <sup>6</sup>Saint-Venant Laboratory for Hydraulics, Chatou, France.

11 <sup>7</sup>CETU Elmis Ingénieries, University of Tours, Chinon, France.

12 <sup>8</sup>EDF, Centre Ingénierie Hydraulique, La Motte Servolex, France.

13 *Correspondence to:* Jules Le Guern (leguern@univ-tours.fr).

## 14 Abstract

15 **Despite the inherent difficulties to quantify its value, bedload transport is essential to understand fluvial**  
16 **systems. In this study, we assessed different indirect bedload measurement techniques with a reference**  
17 **direct bedload measurement in a reach of a large sandy-gravel bed river. Acoustic Doppler Current Profiler**  
18 **(aDcp), Dune Tracking Method (DTM) and hydrophone measurement techniques were used to determine**  
19 **bedload transport rates by using calibration with the reference method or by using empirical formulas.**  
20 **Results show that the hydrophone is the most efficient and accurate method to determine bedload fluxes**  
21 **in the Loire River. Although further work is needed to identify the parameters controlling sediment self-**  
22 **generated noise, the calibration procedure adopted in this study allows a satisfactory estimation of**  
23 **bedload transport rates. Moreover, aDcp and hydrophone measurement techniques are accurate enough,**  
24 **to quantify bedload variations associated to dune migration.**

## 25 1. Introduction

26 Worldwide, rivers are in crisis (Vorösmarty et al., 2010). While changes in flow characteristics and fragmentation  
27 are well known (Grill et al., 2019), the impacts of human activities on the sediment budgets are yet  
28 underrepresented (Kondolf et al., 2018). The quantification of bedload transport is a key element to understand,  
29 manage and restore the physical and ecological functioning of fluvial systems. It is a prerequisite to an accurate  
30 estimation of global sediment budgets delivered by rivers to oceans (Syvitski and Milliman, 2007), to better  
31 understand bedform dynamics in river channels (Best, 1988; Bertoldi et al., 2009; Rodrigues et al., 2015; Claude

Supprimé: section

Supprimé: Even though parameters controlling self-generated noise of sediments still need to better understood

Supprimé: determined

Supprimé: good approximation

Supprimé: both able

Supprimé: continuously measure

Supprimé: transport

Supprimé: bedform

Supprimé: Vorösmarty

Supprimé: is

Supprimé: constitutes

Supprimé: the

46 et al., 2014) and to reproduce satisfactorily morphodynamic processes with numerical modelling (Mendoza et al.  
47 2017; Cordier et al., 2020).

48 However, in large rivers, this parameter remains difficult to estimate mainly due to human and material resources  
49 required to collect accurate measurements. Among the available tools, indirect measurement techniques are  
50 promising alternatives, to direct measurements that are often cumbersome to implement, and can be time-  
51 consuming and perilous (Gray et al., 2010). Since the 2000s, numerous studies were proposed to process the  
52 signal captured by acoustic Doppler current profilers (aDcp) as a tool for determining the apparent bedload velocity  
53 (Rennie et al., 2002; Rennie and Villard, 2004; Rennie and Millar, 2004; Kostaschuk et al., 2005; Villard et al.,  
54 2005; Gaeuman and Jacobson 2006; 2007; Holmes et al., 2010; Ramooz and Rennie, 2010; Latosinski et al., 2017;  
55 Conevski et al., 2019; Conevski et al., 2020a). The use of passive acoustic instruments has also been widely used

56 to quantify bedload transport. Even though these latter techniques have been developed through the application of  
57 measurement tools such as geophones or hydrophones, their domain of applicability is restricted to the study of  
58 rivers with coarse sediments (Barton et al., 2010; Hilldale et al., 2014; Marineau et al., 2016; Geay et al., 2017).

59 In sandy-gravel bed rivers, the presence of bedforms is generally used to indirectly estimate bedload transport  
60 (Simons et al., 1965). Single beam (Peters, 1978; Engel and Lau, 1980) or multibeam echosounders (Nittrouer et  
61 al., 2008; Leary and Buscombe, 2020) are techniques tools usually adopted to determine morphological parameters  
62 (such as bedform height, wavelength and celerity) or to estimate sediment budget (Frings et al., 2014). These  
63 bathymetrical surveys are often carried out simultaneously with sediment sampler measurements (Gaeuman and  
64 Jacobson, 2007; Claude et al., 2012) to calibrate the signal with a direct reference although the latter are intrusive  
65 and characterized by a low spatial representativeness. These drawbacks can therefore limit the applicability of  
66 these measurement techniques, in particular for large lowland rivers.

67 In this work, we compare the efficiency of active and passive acoustic techniques to quantify bedload transport.  
68 The investigation took place in a reach of the Loire River (France), which is characterized by the presence of  
69 migrating bars and superimposed dunes (Le Guern et al., 2019b).

70 The main objectives of this study were: 1) to compare indirect methods for estimating bedload with bedload  
71 estimates based on physical samples; 2) to estimate the accuracy of acoustic methods to measure cross sectional  
72 variations of bedload fluxes for various discharge conditions; and 3) to investigate the capabilities of hydrophones  
73 and aDcps at capturing bedload variations along bedforms.

## 74 2. Study site

75 The study site is located near Saint-Mathurin-sur-Loire, in the lower reach of the Loire River (France), approximately  
76 150 km upstream of the mouth of the Loire River. The study reach is 2.5 km long, 500 m wide, nearly straight, with  
77 a bed slope of 0.02 % (Fig. 1). The riverbed is composed of a mixture of siliceous sands and gravels with a median

Supprimé: the

Supprimé: correctly quantify its measurement.

Supprimé: (Gray et al., 2010)

Supprimé: ).

Supprimé: but

Supprimé: -sizes

Supprimé: standard

Supprimé: used

Supprimé: Moreover, t

Supprimé: acoustic measurements

Supprimé: In this work, we compare the efficiency of active (aDcp, echosounder) and passive (hydrophone) acoustic techniques is assessed for the quantification of bedload transport in a reach of the Loire River (France), which is characterized by the presence of migrating bars and superimposed dunes (Le Guern et al., 2019b).

Supprimé: to compare indirect measurements techniques with a direct measurement technique commonly employed in large sandy-gravel bed rivers (isokinetic samplers) at determining bedload sediment transport rates

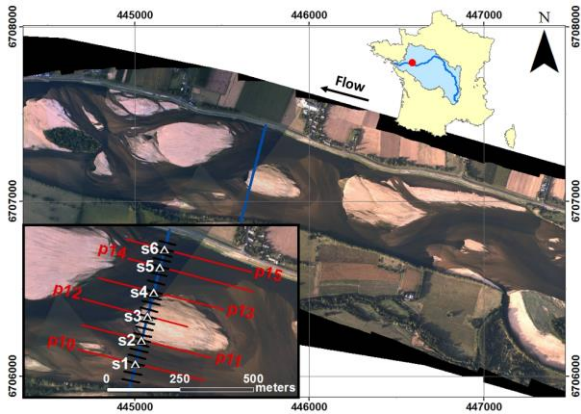
Supprimé: to estimate the capacity of acoustic signals to detect the bedload axes on relatively wide cross-sections for various discharge conditions

Supprimé: for

Supprimé: transport on

103 diameter ( $D_{50}$ ) of 0.9 mm. It varies between 0.3 and 3.1 mm with a standard deviation of 0.4 mm. The 90<sup>th</sup> percentile  
 104 of the sediment grain size distribution ( $D_{90}$ ) is variable with a median value of 3.3 mm varying from 0.5 to 15.7 mm.  
 105 Hydraulic conditions at the sampling points varied with discharge and the median water depth and water velocity  
 106 are 1.6 m and 0.9 m.s<sup>-1</sup> respectively. The width-to-depth ratio ranges from 120 to 550 depending on discharge  
 107 variations. The mean annual discharge at the Saumur gauging station (approx. 30 km upstream) is 680 m<sup>3</sup>.s<sup>-1</sup>, with  
 108 a 2-years flood of 2700 m<sup>3</sup>.s<sup>-1</sup>. Surveys were conducted during various hydrological conditions, with flow discharges  
 109 ranging from 200 to 2400 m<sup>3</sup>.s<sup>-1</sup> (Fig. 2a).

110 Bars are characterized by an average wavelength of 1300 m, corresponding to approximately three times the  
 111 channel width. The mean bar height is 1.5 m. At submerged conditions, bars can migrate with a celerity of 0.5 to 2  
 112 meters per day. During floods, the bar celerity can increase up to 4 meters per day (Le Guern et al., 2019a). During  
 113 floods, dunes are superimposed to bars, whose height, wavelength and mean celerity are approximately of 0.3 m,  
 114 4.4 m and 32 meters per day, respectively.



115  
 116 Fig. 1: Aerial photographs of the study site in 2017 (courtesy of Dimitri Lague, University of Rennes, France) with  
 117 location of sampling points (white triangles) on the sediment transport gauging cross section (blue line), bathymetric  
 118 profiles (red lines) and hydrophone drifts (black lines).

### 119 3. Materials and methods

120 Direct measurements of bedload sediment transport rates were performed using pressure- difference samplers.  
 121 This conventional approach was used to evaluate three indirect acoustic methods: the apparent bedload velocity  
 122 assessed from aDcp measurements, the dune tracking method (DTM) inferred using single-beam echosounding,  
 123 and the self-generated noise (SGN) of sediments measured using a hydrophone. A total of 72 surveys were

Supprimé: much

Supprimé: return period equal to

Supprimé: view

Supprimé: theoretical

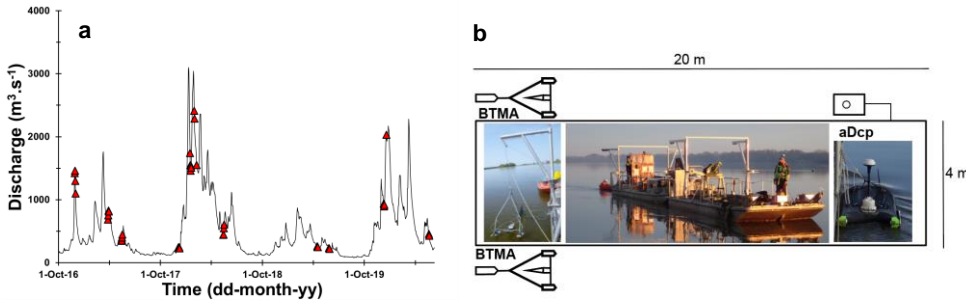
Supprimé: isokinetic

Supprimé: samplers (BTMA, see below) adopted here as reference

Supprimé: classical

Supprimé: retained

133 performed from October 2016 to May 2020 (discharge ranging between 210 m<sup>3</sup>.s<sup>-1</sup> and 2290 m<sup>3</sup>.s<sup>-1</sup>) including 43  
 134 surveys with isokinetic samplers presented on Fig. 2a.



135  
 136 Fig. 2: (a), distribution of surveys along the hydrograph of Saumur gauging station located about 30 km upstream the  
 137 study site. (b), Scheme of the main boat and disposition of monitoring facilities.

138 **3.1. Bedload rates obtained using isokinetic samplers**

139 Bedload transport rates were measured using two synchronized Bedload Transport Meter Arnheim (BTMA)  
 140 samplers, consisting on a sampling basket mounted on a frame. The sampling basket have a rectangular mouth of  
 141 0.05 m high and 0.085 m wide. Complete description of the sample can be found in de Vries (1979) or in Eijkelkamp  
 142 (2003). Devices were mounted on a 20 meter-long boat stabilized using two anchors (Fig. 2b). These two samplers  
 143 were deployed on 6 sampling points (S1 to S6) distributed along a cross section (Fig. 1). At each sampling point,  
 144 10 samples were collected with each BTMA (20 in total) and volumes of each samples were measured in situ with  
 145 a graduated cone (Imhoff cone). Collected volumes were integrated over at least 2 minutes. All samples volumes  
 146 from each BTMA were merged for sieving analysis (leading to 2 sediment samples per sampling point; one for  
 147 each BTMA). Then, the average volume of caught sediments from the 2 BTMAs was computed and converted into  
 148 instantaneous unit bedload rates as follow.

$$149 q_{s,BTMA} = \frac{V}{b} \alpha \varepsilon \rho_s \times 10^3; \quad (1)$$

150 where  $q_{s,BTMA}$  is the unit bedload transport rate (g.s<sup>-1</sup>.m<sup>-1</sup>),  $\alpha$  is the trap efficiency factor based on calibration ( $\alpha=2$ ),  
 151  $V$  is the mean volume of the instantaneous sediment catch (m<sup>3</sup>.s<sup>-1</sup>),  $b$  is instrument's mouth width ( $b=0.085$  m),  $\rho_s$   
 152 is the sediment density (2650 kg.m<sup>-3</sup>) and  $\varepsilon$  is the volumetric sediment concentration (assumed to be equal to 0.65).  
 153 Suggested values of  $\alpha$  and  $b$  were adopted from Boiten (2003) which mentioned that the trap efficiency factor not  
 154 include the possible losses of sediment finer than 0.3 mm (mesh size opening). Sampler positions and sampling  
 155 quality were controlled by using two cameras mounted on the BTMAs but records during flood events were  
 156 unusable because of increasing water depth and suspension. Sediment samples were analysed using the standard  
 157 sieving technique (Folk and Ward, 1957) to determine the grain size distribution (GSD) using the tool "GRADISTAT"

Supprimé: isokinetic

Supprimé: . Samplers consists of

Supprimé: so

Supprimé: -

Supprimé: using Eq. (1)

Supprimé: On each sampling point, collected BTMA values were integrated over at least 2 minutes. The unit bedload rate for each sampling point was obtained by averaging the volumes of sediment collected using Eq. (1):

Supprimé: the width of the mouth of the instrument

Supprimé: volumetric mass of sediment

Supprimé: This calibration factor come from successive calibration procedures concluding to the same calibration coefficient of 2.

172 developed by Blott and Pye (2001). Uncertainties associated to the estimation of the unit bedload were calculated  
173 following Frings and Vollmer (2017).

### 174 3.2. Apparent bedload velocity from aDcp

175 Simultaneously with the BTMA measurements, an aDcp was installed on the boat (Fig. 2b). Measurements were  
176 performed using a Sontek Riversurveyor M9 (bi-frequency, 1 and 3 MHz) or a Teledyne RD Instruments Rio Grande  
177 (1.2 MHz). The sampling time needed to get a stable apparent velocity is in the range 3 min for the case without  
178 bedforms (Conevski et al., 2019) and 25 min (Rennie et al., 2002). In our study the sampling time range was,  
179 between 5 and 190 minutes. The aDcp was coupled with a RTK GPS Magellan ProFlex 500 receiving position  
180 corrections via the Teria network (centimeter level accuracy). The aDcp measurement allowed the use of both  
181 empirical approach and calibration approach for comparison with sediment sampler measurements. The apparent  
182 bedload velocity  $V_a$  was estimated from the bottom tracking signal, allowing the identification and the position of  
183 the river bed. In case of mobile bed, the Doppler shift of the backscattered acoustic pulse of the bottom track  
184 depends on to the boat velocity and to the bed velocity. According to Rennie et al. (2002), the apparent bedload  
185 velocity can be estimated using:

$$186 V_a = V_{GPS} - V_{BT}; \quad (2)$$

187 where  $V_{GPS}$  and  $V_{BT}$  are the boat velocity according to GPS reference and bottom track respectively. When the  
188 GPS signal was poor or missing, the apparent velocity was considered to be equal to the boat velocity according  
189 to bottom track reference because measurements were performed in a static position (representing 15% of the  
190 dataset). Following Jamieson et al. (2011), the apparent velocity  $V_a$  was calculated for the North and East velocity  
191 components (respectively  $\vec{V}_{aE}$  and  $\vec{V}_{aN}$ ), limiting the over estimation especially in areas where inconsistent

192 directions and low magnitudes of bedload velocity were found:  $V_a = \sqrt{V_{aE}^2 + V_{aN}^2}$ .

193 To avoid compass and GPS issues, and to eliminate the effect of residual lateral displacement of the anchored  
194 boat, the apparent bedload velocity was projected onto the flow direction using:

$$195 V_{a\ proj} = V_a \cdot \cos\left(\frac{w_{dir\ BT} - b_{dir\ BT}}{180} \cdot \pi\right); \quad (3)$$

196 with  $w_{dir\ BT}$  the flow direction with bottom track reference and  $b_{dir\ BT}$  the boat direction with the bottom track reference  
197 (in degree). Equation (3) gives a value of apparent bedload transport velocity for each time step (approximately  
198 equal to 1 s) that was averaged to obtain a value for each sampling point. This method assumes that bedload is  
199 orientated in the same direction than the main flow. According to Rennie et al. (2002), the bedload transport rate  
200 per unit width ( $q_s\ ADCP$ ,  $g \cdot s^{-1} \cdot m^{-1}$ ) can be computed from two different kinematic models, namely:

$$201 q_s\ ADCP = \frac{4}{3} \rho_s r V_{a\ proj}^2 \times 10^3; \quad (4)$$

- Supprimé: The u
- Supprimé: y
- Supprimé: of
- Supprimé: was
- Supprimé: using the equation of the stochastic uncertainty from
- Supprimé: two aDcps were positioned
- Supprimé: not well defined and ranging between
- Supprimé: in
- Supprimé: Sampling
- Supprimé: d
- Supprimé: A
- Supprimé: were
- Supprimé: that allow

- Supprimé: respectively
- Supprimé: directly

- Supprimé:  $V_{aE}$
- Supprimé:  $V_{aN}$
- Supprimé: giving better results
- Supprimé:  $V_{aE}^2$
- Supprimé:  $V_{aN}^2$

- Supprimé:  $V_{a\ proj} = V_a \cdot \cos\left(\frac{w_{dir\ GPS} - b_{dir\ BT}}{180} \cdot \pi\right);$
- Supprimé: GPS
- Supprimé: water
- Supprimé: GPS
- Supprimé: Eq.
- Supprimé: about
- Supprimé: involve the assumption
- Supprimé: direction
- Supprimé:  $V_a$

232 where  $r = D_{50}/2$  is the particle radius,  $D_{50}$  is the median sediment diameter (m),  $\rho_s$  is the sediment density (2650

233 kg.m<sup>-3</sup>). In this model, it is assumed the maximum bedload thickness is a single particle and:

234  $q_s ADCP = V_{a\ proj} d_s c_b \rho_s$  (5)

235 where  $c_b$  is the concentration of the active transport layer considered as the saltation height (van Rijn, 1984) and

236 the van Rijn (1984) formulation was adopted to compute the active layer thickness ( $d_s$ ) as a function of the hydraulic  
237 condition and sediment grain size:

238  $d_s = 0.3 D_s^{0.7} T^{0.5} D_{50}$  (6)

239  $c_b = 0.18 \frac{T}{D_s} c_0$  (7)

240  $T = \frac{(\bar{u}')^2 - (u_{cr}')^2}{(u_{cr}')^2}$  (8)

241  $\bar{u}' = \frac{5.75 \log\left(\frac{12d}{3D_{90}}\right)}{u}$  (9)

242 where  $c_0$  is the maximum bedload concentration (0.65),  $T$  is the transport stage parameter that reflects the  
243 sediment mobility,  $\bar{u}'$  is the bed shear velocity related to the grain (m.s<sup>-1</sup>),  $d$  is the mean water depth (m),  $\bar{u}$  is the  
244 mean flow velocity measured from the aDcp (m.s<sup>-1</sup>) and  $u_{cr}$  is the critical bed shear velocity (m.s<sup>-1</sup>) calculated from  
245 the Shields curve (Van Rijn, 1984) and function of grain size through the scaled particle parameter  $D$ :

246  $D = D_{50} \left[ \frac{(s-1)g}{v^2} \right]^{\frac{1}{3}}$  (10)

247 where  $g$  is the acceleration of the gravity (m.s<sup>-2</sup>),  $v$  is the kinematic viscosity (m<sup>2</sup>.s<sup>-1</sup>) and  $s$  the sediment density  
248 ratio. For the range of grain size of this study,  $u_{cr}$  is computed as follows:

249  $10 < D \leq 20$ ;  $u_{cr} = [0.04 D^{-0.1} (s-1)gD_{50}]^{0.5}$  (11)

250  $20 < D \leq 150$ ;  $u_{cr} = [0.013 D^{0.29} (s-1)gD_{50}]^{0.5}$  (12)

251 In order to evaluate the sensibility of the apparent bedload post-processing, the two kinematic models (Eq. 4 and  
252 Eq. 5) were tested using raw apparent bedload velocity ( $V_n$ ) and projected apparent bedload velocity ( $V_{a\ proj}$ ).

253 To assess the capability of the aDcp to detect bedforms through the evolution of apparent bedload velocity, 3  
254 surveys were conducted by positioning the aDcp 0.6 m above the river bed. This experimental scheme was adopted  
255 to avoid lateral movements of the boat, to be as close as possible to the river bed, and to reduce the space between  
256 beams. This configuration permitted to fix the footprint for each beam to about 0.0046 m<sup>2</sup> and a distance of 0.56 m  
257 between opposed beams. This allowed to describe the apparent bedload velocity with a finer accuracy especially  
258 in the presence of bedforms of 0.2 m height and 3.9 m long (in average). These surveys were performed for several  
259 hours (from 2.1 h to 4.7 h) to capture the migration of more than one dune lee side pass under the device. The  
260 value of apparent bedload velocity was smoothed by using a moving windows with an average of 500 points

Supprimé: W

Supprimé:  $\rho_s$ ; . . . . . (5)  
In Eq. (4),

Supprimé: and the active layer thickness ( $d_s$ ) is considered as a constant, with

Supprimé: .

Supprimé: In Eq. (5),  $\lambda$

Supprimé: is the porosity of the active transport layer considered as a constant and equal to 0.35,

Supprimé:  $d_s = \frac{0.3 D_s^{0.7} T^{0.5}}{D_{50}}$

Mis en forme

Mis en forme

Mis en forme

Mis en forme

Supprimé: where

Supprimé:  $D_{90}$  is the 90<sup>th</sup> percentile of the sediment grain size (m)

Supprimé: .

Supprimé: water

Supprimé: insonified surface...ootprint for each beam to about 0.0046 m<sup>2</sup> and a distance of 0.56 m between opposed beams. This allowed to describe, and could allow a better understanding of...the apparent bedload velocity with a finer accuracy especially in the presence of bedforms of 0.2 m height and 3.9 m long (in average).gradient along bedforms (...)

Supprimé: during ...or several hours (from 2.1 h to 4.7 h) to see (...)

Supprimé: a

306 (approximately 500 seconds) to remove the outliers from the raw dataset. In the present study, all negative values  
307 were excluded from the comparison with BTMA measurements (16% of apparent velocity values).

Supprimé: noise

### 308 3.3. Bathymetrical echosounding and dune tracking method

309 A single beam echosounder Tritech PA500 (0.5 kHz) coupled with a RTK GPS LEICA Viva GS25 were used for  
310 high-frequency bathymetric surveys to determine bar and dune morphodynamics along 6 longitudinal profiles  
311 (about 400 m long) centred on sampling points indicated in Fig. 1. Dune height ( $H_D$ ) and wavelength ( $\lambda_D$ ) were  
312 estimated using the Bedform Tracking Tool (BTT) based on the zero-crossing method (Van der Mark and Blom,  
313 2007). Dune celerity ( $C_D$ ) was estimated with the Dune Tracking Method (DTM, Simons et al., 1965; Engel and  
314 Lau, 1980) following the dune crests between two subsequent bathymetric surveys for a mean interval time equal  
315 to 40 minutes. The interval time needs to be adjusted with discharge because of the dune celerity variation from  
316 one survey to another. The determination of a proxy to evaluate sediment transport directly from DTM  
317 measurements is difficult because dune migration is function of several parameters. A semi-empirical equation that  
318 accounts for these parameters was used to compare bedload transport rates with the reference measurement. The  
319 computed dune parameters were used to calculate the unit bedload transport rate ( $q_s^{DTM}$ , g.s<sup>-1</sup>.m<sup>-1</sup>) using the  
320 formula by Simons et al. (1965):

Supprimé: integer

$$321 q_s^{DTM} = (1-\lambda) \rho_s H_D C_D \beta \times 10^3; \quad (13)$$

322 where  $H_D$  is the mean dune height along the profile (m),  $C_D$  is the median dune celerity (m.s<sup>-1</sup>) and  $\beta$  is the bedload  
323 discharge coefficient equal to 0.5 for a perfect triangular dune shape. The  $\beta$  coefficient neglects the volume of  
324 bypassing material from previous dunes or exchanges between bedload and suspended load (Wilbers, 2004). Due  
325 to its large variability (Van den Berg, 1987; Ten Brinke et al., 1999; Wilbers, 2004), the sensibility of the bedload  
326 transport rate was assessed for  $\beta=[0.33; 0.57]$ , as proposed by Engel and Lau (1980) and Wilbers (2004).  
327 Considering the accuracy of the bathymetrical echosounding relative to the dune size, the sinuosity of dune crests,  
328 and the representativeness of dune celerity, only profiles with a mean dune height greater than 0.1 m and more  
329 than 10 dunes were considered.

Supprimé: in the literature (

Supprimé: ,

Supprimé: ;

Supprimé: ,

Supprimé: of

Supprimé: are

### 330 3.4. Hydrophone and acoustic power

331 Passive acoustic monitoring was performed with a Teledyne RESON Hydrophone TC4014-5 (sensitivity of -180  
332 dB) plugged into an EA-SDA14 card from RTSYS Company. This device has a large frequency range from 0.015  
333 to 480 kHz, with a linear response until 250 kHz ( $\pm 3$ dB). The beam-pattern of the hydrophone is omnidirectional.  
334 The hydrophone has been deployed following the protocol proposed by Geay et al. (2020). Longitudinal profiles  
335 were defined on the sediment transport sampling section (22 see Fig. 1). The boat was positioned upstream the  
336 sediment transport gauging section and left adrift at flow velocity. Depending on the water depth, the hydrophone

Supprimé: A total of 22 |

Supprimé: was

Supprimé: gauging

Supprimé: directly

349 was installed at a constant depth between 0.4 and 0.7 m below the water surface. Data acquisition was stopped  
 350 after the boat crossed the sediment transport gauging section. The drift duration ranged between 15 to 140  
 351 seconds, depending on the flow velocity (mean time of 31 s). For each drift, a spectral probability density (SPD)  
 352 was computed (Merchant et al., 2013). Then, a median Power Spectral Density (PSD) was computed as proposed  
 353 by Geay et al. (2017). Median PSD are preferred to mean PSD as it enables to filter anomalous acoustic events  
 354 such as the hydrophone impinging the riverbed. The acoustic power ( $P$ ) for each drift was computed by integrating  
 355 the median PSD over a range of frequency comprised between  $f_{min}$  (15 kHz) and  $f_{max}$  (350 kHz) (Geay et al., 2020):

$$356 P = \int_{f_{min}}^{f_{max}} PSD(f) df; \quad (14)$$

357 The minimum frequency was chosen to avoid hydrodynamic and engine noises, while the maximum frequency was  
 358 set by the upper limit frequency of the device and was adjusted related to  $PSD$ . Finally, the nearest hydrophone  
 359 drift for each BTMA sampling point was selected. Hydrophone drifts and sampler measurements were not  
 360 synchronized. Several tests were carried out to ensure that these acoustic power variations were not related to the  
 361 distance between the hydrophone and the river bed. As no theoretical expression has been developed to estimate  
 362 bedload rates from hydrophone measurements, only the calibration approach was implemented.

## 363 4. Results

### 364 4.1. Comparison between acoustics and direct bedload transport rate measurements

365 The BTMA dataset is composed of 135 unit bedload rates calculated from 2628 individual sediment samples. This  
 366 dataset represents an average of 19 samples on each sampling point to compute unit bedload rates (minimum of  
 367 5 and maximum of 57 samples). Bedload rates measured using the BTMAs ranged between 0.01 and 268  $g \cdot s^{-1} \cdot m^{-1}$ .  
 368 The standard deviation of unit bedload rates increased with discharge with a mean value of 33  $g \cdot s^{-1} \cdot m^{-1}$ . This  
 369 illustrates the spatio-temporal variability of sediment transport induced by bedform migration.

370 The aDcp dataset is composed of 96 simultaneous measurements of apparent bedload velocity and BTMA  
 371 samplings (Fig. 3a). The mean apparent bedload velocity is 0.02  $m \cdot s^{-1}$  and the maximum value was 0.11  $m \cdot s^{-1}$ . A  
 372 Reduced Major Axis (RMA) regression has been computed between these two variables with a coefficient of  
 373 determination (COD)  $R^2$  equal to 0.51:

$$374 q_s = \sqrt{1456} V_a - 2.44; \quad (15)$$

375 As shown in Fig. 3a, this site-specific calibration procedure at a reach of the Loire River describes fairly well the  
 376 dataset already published on several world large rivers, (Rennie et al., 2017).

Supprimé: , so

Supprimé: determined

Supprimé: done

Supprimé: rare and powerful

Supprimé: are

Supprimé: formula

Supprimé: sampling

Supprimé: That

Supprimé: 98

Supprimé: 0.022

Supprimé: 48

**Commenté [J1]:** We decided to change this equation, 1) because of the modification of Eq.3; 2) because the linear regression have a better COD and allow a comparison with other calibration equations of Rennie et al. (2017).

Supprimé: 3545

Supprimé:  $V_a^{0.25}$

Supprimé:

Supprimé: is in good agreement with the Rees, Missouri and Fraser rivers

Supprimé: The RMA regression presented here describes fairly well the dataset already published on several world large rivers.

Supprimé: It also suggests that the experimental relationship between  $V_a$  and  $q_s$  BTMA is similar for similar material (in terms of grain size).



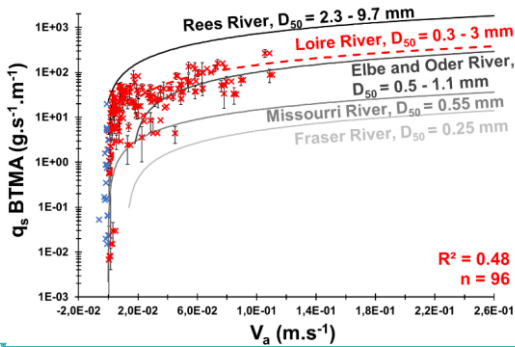
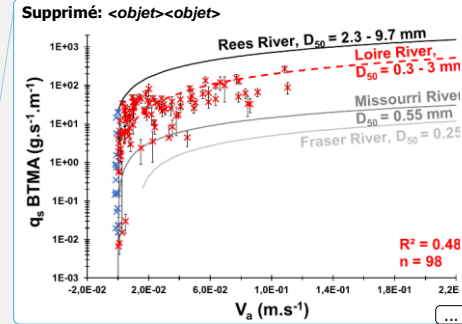


Fig. 3: unit bedload transport rates measured with BTMA samplers as a function of the apparent bedload velocity measured with aDcp. Red dashed line represents the RMA regression of the Loire River. Comparison with other site-specific calibration curves (Conevski et al., 2020a; Rennie et al. 2017). Blue marks represent negatives apparent bedload velocity excluded from this regression.

To evaluate the accuracy of a method against a reference, the discrepancy ratio is classically employed in the literature (Van Rijn, 1984; Van den Berg, 1987; Batalla, 1997), and is defined as the ratio between the bedload rate estimated with the indirect method and the bedload rate using BTMA. Computed bedload layer volume concentration (Eq. 7) varies between 0.005 and 0.1 (0.03 in average). Bedload layer thickness ( $d_s$ ) (Eq. 6) ranges between  $1D_{50}$  and  $7D_{50}$  ( $5D_{50}$  in average). Bedload rates computed using Eq. (5) underestimate BTMA bedload rates with only 24% of the dataset in the discrepancy ratio (Figure 4b). By considering apparent bedload velocity without projection onto the flow direction, the kinematic model (Eq. 5) estimates satisfactorily BTMA bedload rates with 41% of the dataset in the discrepancy ratio. Conversely, using raw apparent bedload velocity in Eq. (4), leads to only 33% of the dataset in the discrepancy ratio against 54% with projected  $V_{\beta}$ . According to these results, Eq. (4) better describes the sampler bedload rates with projected apparent bedload velocity whereas raw apparent bedload velocity are preferred with Eq. (5). Some outlier data are observed for BTMA bedload discharge lower than  $0.1 \text{ g.s}^{-1}.\text{m}^{-1}$ . These points correspond to low flow conditions for which bedload samplers could under-estimate bedload fluxes (gap between the sampler mouth and the riverbed).



Supprimé: (a),

Supprimé: (b), log/log correlation between bedload rates measured with BTMA sampler and calculated using Eq. (4) and Eq. (5). Solid black line represents the perfect

Supprimé: Bedload transport rates were calculated considering the concentration and the thickness of active layer as constant.

Supprimé: In order t

Supprimé: . This ratio

Supprimé: over

Supprimé: better

Supprimé: the

Supprimé: uation

Supprimé: the

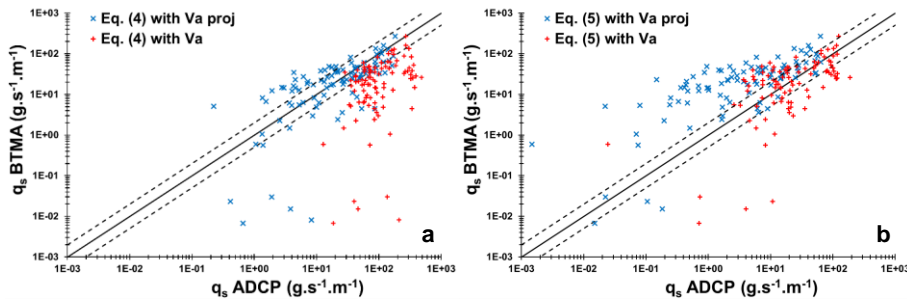
Supprimé: uation

Supprimé: the

Supprimé: uation

Supprimé: more significant

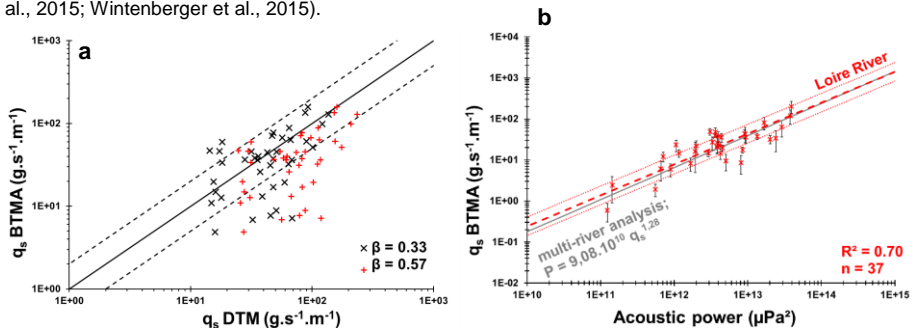
Supprimé: Approximately 57% of the computed bedload transport rate (Eq. 4) is within the discrepancy ratio (Figure 3b), while only 14% when using the Van Rijn definition of the



456  
457 Fig. 4: log/log correlation between bedload rates measured with BTMA sampler and calculated using a) Eq. (4) and; b)  
458 Eq. (5). Solid black line represents the perfect correlation and dashed black lines represents a factor of 2 above and  
459 below the perfect correlation.

460 It appears difficult to estimate bedload rates only from dune celerity by assuming a direct relation between dune  
461 celerity and bedload transport rates measured with BTMA. Estimation of bedload transport rates from dune  
462 morphology has been performed by using empirical formula of Simons et al. (1965) (Eq. 13). The dataset is  
463 composed of 49 DTM profiles with associated BTMA samples. The mean dune height and length vary from 0.1 to  
464 0.5 m, and 1.3 to 12 m, respectively. The median dune celerity varies between 13 and 61 m.d<sup>-1</sup>. According to Fig.  
465 4a, bedload rates estimated with a discharge coefficient  $\beta = 0.33$  are in agreement with BTMA bedload rates with  
466 67% of values in a factor of 2 of the perfect correlation compared with 49% of values for a discharge coefficient of  
467 0.57 (Fig.5a). The definition of the discharge coefficient proposed by Engel and Lau (1980) is better adapted for  
468 the observed dune shapes found in the Loire River which are characterized by mean steepness ( $H_D/L_D$ )  
469 approximately equal to 0.05 (in line with other observations on the Loire River, Claude et al., 2012; Rodrigues et  
470 al., 2015; Wintenberger et al., 2015).

- Supprimé: making
- Supprimé: of
- Supprimé: values in a factor 2, whereas 49%
- Supprimé: ,
- Supprimé: definition of the discharge coefficient
- Supprimé: of
- Supprimé: of



471  
472 Fig. 5: log/log correlation between bedload rates measured with BTMA samplers and bedload rates calculated using  
473 Eq. (13). Solid black line represents the perfect correlation and dashed black lines represents a factor of 2 of the perfect

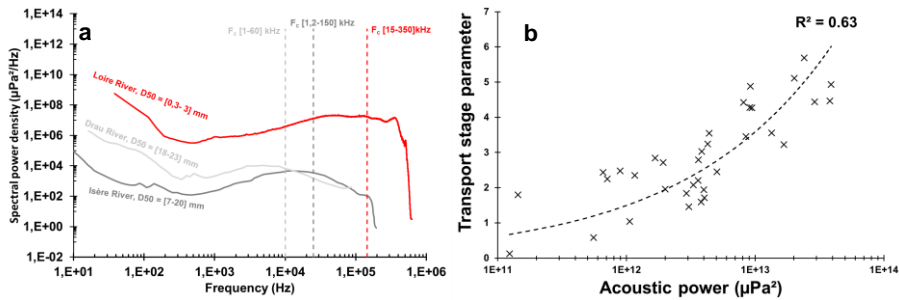
481 correlation b), unit bedload rates measured with BTMA samplers as a function of acoustic power measured with  
 482 hydrophone. Dashed red lines represents the RMA regression with envelopes curves of a factor 2 of the bedload rates.  
 483 Comparison with Geay et al. (2020).

484 Even if the statistical representativeness is lower than other methods (n=37), the RMA regression between the  
 485 acoustic power and BTMA sampling is better ( $R^2=0.70$ ) and 60% of values varying between a factor 2 (Fig. 5b). In  
 486 consequence, new equation to estimate sediment transport from acoustic power is proposed:

$$487 P = 6.6 \times 10^{10} q_s^{1.32}; \quad (16)$$

488 This calibration curve is similar to observations performed by Geay et al. (2020) on 14 study sites distributed on 11  
 489 different rivers despite the use of different instruments (sampler and hydrophone) and the integration of median  
 490 PSD over a wider range of frequency in the present study. Moreover, the median PSD differ from the Isère River  
 491 (Petrut et al., 2018) and from Drau River (Geay et al., 2017). These rivers are characterised by coarser sediments  
 492 (see Fig. 6a) and the central frequency of the PSD are decreasing for an increasing  $D_{50}$ . These observations are  
 493 in line with Thorne's (1986) theory. The central frequency of the median spectrum of the Loire River is approximately  
 494 equal to 140 kHz. The frequency band of the bedload is shifted towards high frequencies due to finer grain size.

495 The acoustic power corresponding to the integration of the spectrum over a range of frequency is related to the  
 496 grain size (Thorne, 1985) and sediment kinematics (Gimbert et al., 2019). To analyse the effect of sediment mobility  
 497 on the acoustic power, the transport stage parameter (Van Rijn, 1984) is calculated. The power law adjusted  
 498 between these two parameters evidences a positive evolution of the acoustic power with sediment mobility (Fig.  
 499 6b).



501 Fig. 6: (a), Comparison of PSD from 3 rivers with varying  $D_{50}$ . (b), transport stage parameter (from Van Rijn, 1984) as a  
 502 function of acoustic power.

503 The comparison can be performed between indirect methods to discuss the acceptability of the BTMA reference.  
 504 The apparent bedload velocity and the acoustic power are poorly correlated with mean dune morphological  
 505 parameters (Table 1).

Supprimé: A

Supprimé: for

Supprimé: about

Supprimé: made

Supprimé: not well-

Supprimé: dune celerity and dune height

Table 1: Coefficient of determination (COD) between dune parameters and acoustic methods (log values).

	P	V <sub>a</sub>	Q <sub>s,BTMA</sub>	H <sub>dune</sub>	C <sub>dune</sub>
H <sub>dune</sub>	0.20	0.27	0.16	-	-
C <sub>dune</sub>	0.22	0.24	0.36	0.22	-

The apparent velocity measures the top layer velocity or dynamical active layer (sediment being transported over a dune), whereas the dune celerity is the mobility of the exchange event active layer, according to Church and Haschenburger (2017). It must be noted that apparent bedload velocity is higher than dune celerity by a factor approximately equal to 100. On the other hand, the apparent bedload velocity is positively correlated with the acoustic power. The COD of the RMA regression is equal to 0.76 (Fig. 7a).

Before focusing on the spatial distribution of unit bedload rates, total bedload rates are calculated by interpolating unit bedload rates between sampling points on the cross section for each method. The COD of the RMA regression established between BTMA bedload rates and water discharge is 0.71 (Fig. 7b) with 77% of the values varying in a factor 2. The dispersion of bedload rates is higher for low water discharge (under mean annual discharge, 800 m<sup>3</sup>.s<sup>-1</sup>). Bedload rates are estimated from Eqs. (13), (15) and (16), for the DTM, the aDcp and the hydrophone, respectively. Both the hydrophone and DTM bedload rates are less scattered with 96% of values in the discrepancy ratio, compared with 82% for the aDcp.

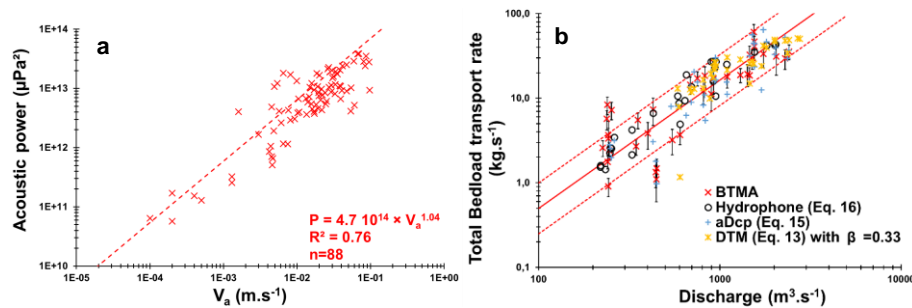


Fig. 7: (a), acoustic power as a function of apparent bedload velocity. (b), Cross section integrated bedload transport rates as a function of discharge.

## 4.2. Spatial distribution of bedload in a sandy gravel-bed river with migrating bedforms

### 4.2.1. Determination of bedload transport on a cross section using acoustics methods

To compare the spatio-temporal distribution of bedload transport rates, sediment transport sampling was performed on the same cross section for all surveys and for various discharge conditions. Two surveys with contrasting discharge conditions and different bed configurations are presented (Fig. 8) to illustrate the capability of acoustics

Supprimé: velocity

Supprimé:

Supprimé: with about a

Supprimé: The aDcp method is measuring the apparent velocity of the grain being transported from the stoss to the lee side of a dune. It must be noted that apparent bedload velocity is higher than dune celerity with about a factor 100, whereas the grain size (D50) is smaller than dune height with the same order. Therefore, sediments that are 100 times smaller than dune height allows the dune migration with a celerity 100 256 times smaller than their own celerity. On the other hand, the apparent bedload velocity is positively correlated with the acoustic power. The RMA regression model explains 76% of the dataset dispersion (Fig. 6a).

Supprimé: explain 71% of the dataset dispersion

Supprimé: Eq.

Supprimé: Eq.

Commenté [J2]: Change is due to modification of Eq. 15

Supprimé: whereas 73

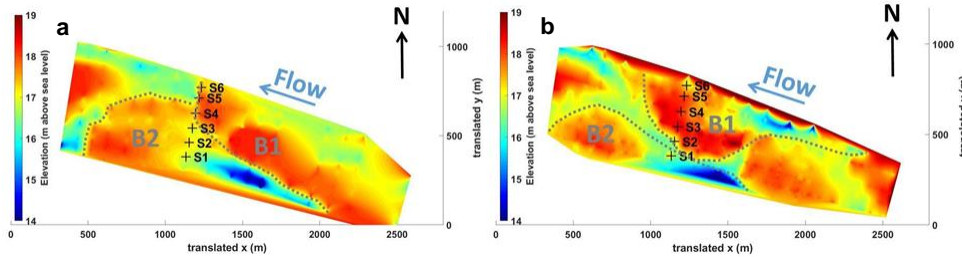
Commenté [J3]: This figure have changed because of the modification of Eq. 15

Supprimé: axes

Supprimé: gauging

Supprimé: capacity

555 methods to determine bedload active width in a river reach characterized by the presence of macroforms and  
 556 superimposed mesoforms (*sensu lato*, Jackson, 1975).



557  
 558 Fig. 8: Bathymetric Digital Elevation Models (obtained using natural neighbours interpolation) showing location of  
 559 sampling points with respect to bar location during: (a), survey of the 17/05/2018 ( $Q=604 \text{ m}^3 \cdot \text{s}^{-1}$ ) and (b), survey of the  
 560 19/12/2019 ( $Q=2050 \text{ m}^3 \cdot \text{s}^{-1}$ ).

561 In May 2018, a bar (B1, Fig. 8a) was located just upstream the sediment gauging section from the center to the  
 562 right part of the channel. In the left part of the channel, BTMA sampling was performed on the stoss side of another  
 563 bar (B2, Fig. 8a). Consequently, bedload rates gradually rose from the center of the channel ( $2 \text{ g} \cdot \text{s}^{-1} \cdot \text{m}^{-1}$ , S4) to the  
 564 left part of the channel ( $15 \text{ g} \cdot \text{s}^{-1} \cdot \text{m}^{-1}$ , S1) except for the DTM (Fig. 9a). The intensity of bedload transport rates was  
 565 evaluated for each acoustic signal from regression equations established above (Eq. 13, 15 and 16, for DTM,  
 566 aDcp and hydrophone, respectively). The linear equation of aDcp calibration allow the calculation of negatives  
 567 bedload flux for apparent bedload velocity below  $0.0016 \text{ m} \cdot \text{s}^{-1}$  (Fig. 9a, S4). ADcp and hydrophone signals followed  
 568 the same trend as the BTMA measurement. In the right part of the channel, no reference measurements were  
 569 available (S5 and S6) but all acoustic signals followed the same trend (increasing bedload transport rates). The  
 570 bedload rates estimated with the DTM were lower than the reference in the left part of the channel. This can be  
 571 explained by the reduced number of dunes in this area that caused a higher uncertainty in dune celerity  
 572 determination. In the right part, the proximity of the bar front induced lower bedload transport rates measured with  
 573 aDcp and hydrophone. DTM integrates sediment dynamics over a longitudinal profile that does not necessarily  
 574 reflect the bedload transport conditions at a local scale. Due to the lee effect provided by the proximity of the bar  
 575 front, dunes were not present downstream of the bar and only dunes located on the stoss side of the bar were used  
 576 to calculate the mean dune celerity. ADcp underestimates whereas the hydrophone method overestimates the unit  
 577 bedload rate compared with BTMA measurements.

Supprimé: axes

Supprimé: bars

Supprimé: done

Supprimé: were

Supprimé: rising

Supprimé: Eq.

Supprimé: Eq.

Mis en forme : Exposant

Supprimé: evolution

Supprimé: there were

Supprimé: whereas hydrophone overestimates BTMA measurements.

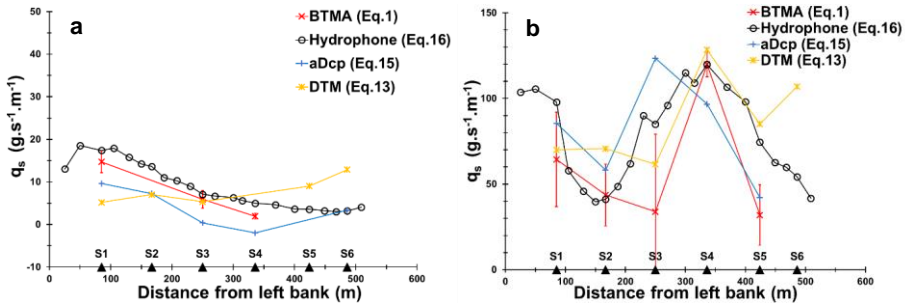
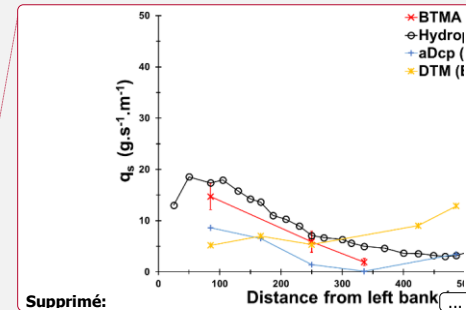


Fig. 9: Lateral distribution of unit bedload rates assessed from different methods for two surveys performed: (a), the 17/05/2018 ( $Q=604 \text{ m}^3\cdot\text{s}^{-1}$ ) and (b), the 19/12/2019 ( $Q=2050 \text{ m}^3\cdot\text{s}^{-1}$ ), respectively.

In December 2019 (Fig. 9b), the flow discharge was higher ( $2050 \text{ m}^3\cdot\text{s}^{-1}$ ) than the value observed in May 2018 ( $Q=604 \text{ m}^3\cdot\text{s}^{-1}$ ) and measured bedload rates ranged between 32 and  $120 \text{ g}\cdot\text{s}^{-1}\cdot\text{m}^{-1}$ . Due to the bar migration, the bed configuration was different. Bar B1 reached the sediment gauging cross section. As a consequence, sampling points S3 to S6 were located on the stoss side of bar B1 (Fig. 8b). The sampling point S2 was located just downstream the bar front where the velocity and sediment transport rates were lower (Fig. 8b). The high spatial resolution of the hydrophone measurements confirmed that the preferential bedload active width was located between 250 and 450 m from the left bank (Fig. 9b). For this survey, acoustic signals (i.e. acoustic power, apparent bedload velocity) followed the same evolution pattern as samplers along the cross section except for S3. Bedload transport rates determined with the DTM did not follow the trend of bedload rates determined with aDcp and hydrophone at the proximity of bar front and near the bank as in the previous survey (S2 and S6). The hydrophone model overestimated the sediment transport in comparison with the BTMAs for S1, S3 and S5.

#### 4.2.2. Sediment transport processes on bedforms analyzed from aDcp and hydrophone

The aDcp computed bedload rates evolved according to bedform location for fixed measurements performed on dunes of height ranging between 0.05 m and 0.2 m (Fig. 10a and 10b). Higher bedload rates values were found on the crest of the dune and lower values in the trough. The amplitude of bedload rates between crest and trough for low flow conditions (Fig. 10b) ranged between  $42 \text{ g}\cdot\text{s}^{-1}\cdot\text{m}^{-1}$  and  $67 \text{ g}\cdot\text{s}^{-1}\cdot\text{m}^{-1}$ . For higher flow conditions, it varied between  $45 \text{ g}\cdot\text{s}^{-1}\cdot\text{m}^{-1}$  and  $91 \text{ g}\cdot\text{s}^{-1}\cdot\text{m}^{-1}$  (Fig. 10a). These values were extracted considering bedload rates in trough as equal to zero (not negative). The aDcp linear regression (Eq. 15) did not allow the calculation of bedload transport rates due to negative apparent bedload velocity. This is the case downstream the lee face of dunes (Fig. 10a, between 8 to 42 min., 96 to 107 min., 185 to 193 min., and 227 to 230 min.; Fig. 10b, between 48 to 55 min. and 153 to 162 min.). The mean time recorded between two successive dune crests was 1 hour.



Supprimé: migrated

Supprimé: on the

Supprimé: axis

Supprimé: isokinetic

Supprimé: about

Supprimé: 9a

Supprimé: 69

Supprimé: 43

Supprimé: 111

Supprimé: 9b

Supprimé: l

Supprimé: 19

Supprimé: -

Supprimé: 104

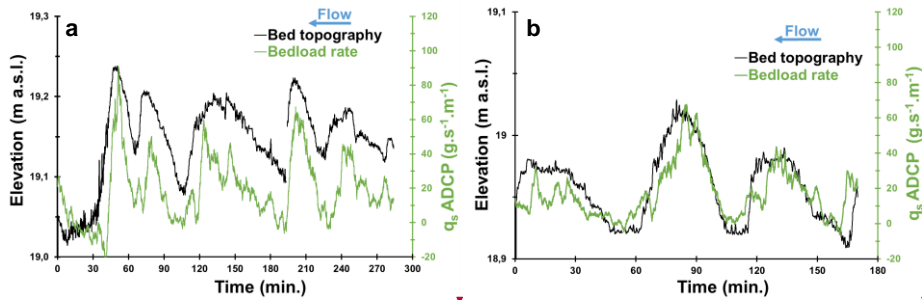
Supprimé: -

Supprimé: -

Supprimé: -

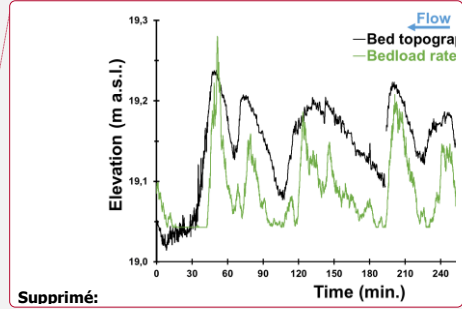
Supprimé: -

Supprimé: -

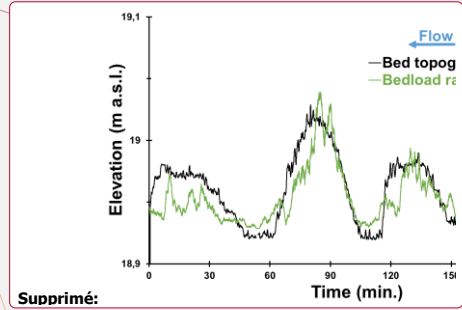


636 Fig. 10: Bedload rates calculated using Eq. (15) and bed topography obtained during a static measurement performed  
 637 using an aDcp. (a), survey done the 20/05/2020 ( $Q=470 \text{ m}^3 \cdot \text{s}^{-1}$ ; mean water depth = 1.04 m) and (b), survey done the  
 638 29/05/2019 ( $Q=210 \text{ m}^3 \cdot \text{s}^{-1}$ ; mean water depth = 0.85 m).

639 Hydrophone drifts showed that the longitudinal evolution of acoustic power can be correlated with changes in  
 640 elevation of the riverbed due to dune and bar presence. For instance, in the presence of a 2 meter high bar front,  
 641 the bedload rate significantly decreased, illustrating the lee effect that is characterised by a decrease in bedload  
 642 sediment transport (Fig. 11a). This shows that the hydrophone is sensitive enough to detect this local phenomenon  
 643 induced by the presence of a bar front immediately upstream. The bedload rates range from about  $8 \text{ g} \cdot \text{s}^{-1} \cdot \text{m}^{-1}$  on  
 644 the bar crest to  $376 \text{ g} \cdot \text{s}^{-1} \cdot \text{m}^{-1}$  in the bar trough ( $1 \cdot 10^{12} \text{ } \mu\text{Pa}^2$  to  $1.7 \cdot 10^{14} \text{ } \mu\text{Pa}^2$  of acoustic power, respectively).  
 645 According to flow velocity measurements, it appears that a 2 m high bar front can influence flow velocity and  
 646 bedload transport rates up to the reattachment point located approximately 100 m downstream. Downstream the  
 647 bar front, the bedload transport rate increased from 11h06min (Fig. 11a) that would be in coincidence with the flow  
 648 reattachment point. Further downstream, the bedload transport rate increased from 8.5 to  $23.4 \text{ g} \cdot \text{s}^{-1} \cdot \text{m}^{-1}$   
 649 (representing respectively an acoustic power of  $1.2 \times 10^{12} \text{ } \mu\text{Pa}^2$  to  $4.1 \times 10^{12} \text{ } \mu\text{Pa}^2$ ), where dunes exhibit a more  
 650 regular shape increasing their amplitudes from 0.02 m to 0.4 m, approximately. On the left part of the channel (Fig.  
 651 11b), the drift was located at the stoss side of a bar where larger dunes were observed (about 1 m in height) with  
 652 superimposed small dunes (height approximately equal to 0.3 m). The bedload transport rate calculated above  
 653 these bedforms increased near the crests of the large dunes (about  $80 \text{ g} \cdot \text{s}^{-1} \cdot \text{m}^{-1}$ ) and decreased in the troughs  
 654 (about  $50 \text{ g} \cdot \text{s}^{-1} \cdot \text{m}^{-1}$ ) where superimposed bedforms were smaller (Fig. 11b).



Supprimé:



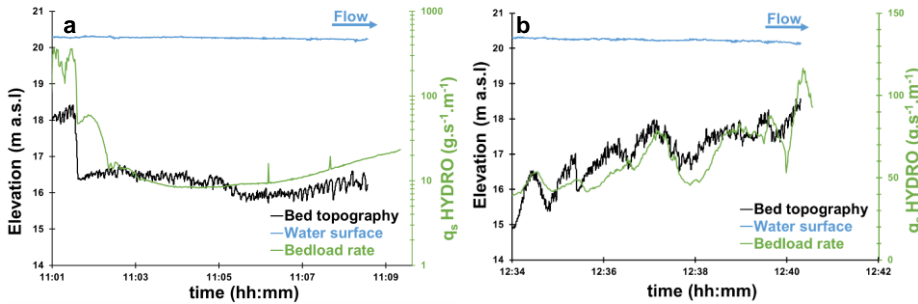
Supprimé:

Supprimé: materialized

Supprimé: , showed

Supprimé: In

Supprimé: on



661  
 662 Fig. 11: Bedload rates calculated on bedforms using the hydrophone and Eq. (16) near a bar front (a) and on a dune  
 663 field (b). Bed topography and water surface along two longitudinal bathymetric profiles for the 08/02/2018 survey,  
 664  $Q=1550 \text{ m}^3\cdot\text{s}^{-1}$ : (a), P10, mean water depth = 3.8 m. The profile length from 11:01 to 11:09 corresponds to 400 m; (b),  
 665 P12, mean water depth = 3.4 m. The profile length from 12:34 to 12:41 corresponds to 518 m.

666 **5. Discussion**

667 **5.1. Relevance of acoustics for computing bedload transport rates**

668 Despite their lack of accuracy and their low spatial representativeness, samplers allow a direct measurement of  
 669 bedload and represents the only reference measurement of bedload in the field. The presence of bars affect  
 670 sediment transport locally and make sampling method very sensitive to the location of the sampling point. For low  
 671 water discharge (below mean annual discharge,  $800 \text{ m}^3\cdot\text{s}^{-1}$ ), bars are emerged and reduce considerably the width  
 672 where sediment transport occurs. The number of sampling points decrease with discharge (because bars were not  
 673 flooded) leading to a higher bedload rates variability (Fig. 7b). Moreover, in weak bedload transport conditions, the  
 674 BTMA sampler most likely performed with reduced efficiency initially calibrated to 50%, (van Rijn and Gaweesh,  
 675 1992; Gaweesh and van Rijn, 1994; Banhold et al., 2016). The presence of dunes influences the performance of  
 676 the sampler by preventing the exact positioning of sampler mouth on the river bed. These deficiencies lead to a  
 677 large uncertainty in bedload estimation which set the limits of the comparison with other methods.

678 The use of hydrophones to estimate bedload transport in a lowland sandy gravel-bed river constitutes a new  
 679 research topic. As discussed by several authors, the use of hydrophones was so far restrained to gravel-bed rivers  
 680 (Bedeus and Ivicsics, 1963; Barton et al., 2010; Hilldale et al., 2014; Thorne, 2014; Marineau et al., 2016; Geay et  
 681 al., 2017) or marine environments (Thorne et al., 1984; Thorne, 1986; Blanpain et al., 2015). More recently, Geay  
 682 et al. (2020) highlighted that the acoustic power measured with a hydrophone can be correlated to the sampler  
 683 measurements of bedload in fluvial environments characterized by bed slopes varying between 0.05 and 2.5% and  
 684 channel width ranging between 8 and 60 m. In these mountainous environments, the median grain size ranged  
 685 between 0.9 and 62 mm (n=582 samples). In our study, the downstream reach of the Loire River shows smaller

- Supprimé: isokinetic
- Supprimé: . To this date
- Supprimé: ,
- Supprimé: the only reference
- Supprimé: based on isokinetic samplers is the only technique used to compare or calibrate another
- Supprimé: sediment gauging method
- Supprimé: large rivers
- Supprimé: for these hydraulic conditions,
- Supprimé: occurs over a very low thickness reducing
- Supprimé: of the sampler (
- Supprimé: Eijkelkamp, 2003

- Supprimé: with
- Supprimé: isokinetic



700 slope ( $S=0.02\%$ ), a wider channel ( $W=500$  m), and a median grain size ranging between 0.3 mm to 3.1 mm ( $n=450$   
701 samples). The hydrophone is therefore an efficient tool for sediment transport gauging, allowing the measurement  
702 of numerous sampling points (average of 17 sampling points) during a relatively shorter time period (one hour).  
703 This high spatial discretization makes the hydrophone functional over a wide range of discharges (even for low  
704 water discharge, Fig. 6b) by catching the high spatial variability of bedload transport. It should be pointed that the  
705 regression calculated in the present study (Eq. 16) is obtained from unit bedload rates (from several samples) and  
706 the acoustic power resulting to a unique acoustical drift, whereas Geay et al. (2020) compared averaged cross  
707 section bedload rates and acoustic power. Despite these differences, the data presented above corroborate the  
708 results by Geay et al. (2020) and support their conclusions concerning the determination of a global calibration  
709 curve between acoustic power and bedload rates by extending its application to the lowland sandy gravel-bed  
710 rivers. Although this need to be confirmed by further investigations to better understand parameters that control the  
711 acoustic power measured (such as the propagation of sound waves in water (Geay et al., 2019) and their  
712 attenuation, the saltation length and associated impact celerity, or sediment grain size), results presented in this  
713 study suggest that the hydrophone method could be an efficient way to measure and to map bedload transport  
714 rates on a wider range of fluvial systems.

715 Several laboratory studies have been carried out (Ramooz and Rennie, 2010; Conevski et al., 2019; Conevski et  
716 al., 2020b) and rivers instrumented with aDcp to determine bedload rates (Rennie et al., 2002; Rennie and Millar,  
717 2004; Gaeuman and Jacobson, 2006; Gaeuman and Pittman, 2010; Brasington et al., 2011; Conevski et al.,  
718 2020a). Recent works have been carried out on two rivers (Elbe, Oder) similar to the Loire River in term of grain  
719 size characteristics, flow and shear velocity, and water depth (Conevski et al., 2020a). Even if the correlation  
720 between apparent bedload velocity and bedload rates is significant, this calibration equation was obtained from two  
721 very similar rivers. Despite these observations, there is no general agreement between bedload rates and apparent  
722 velocity (Rennie and Villard, 2004; Rennie et al., 2017). The response of aDcp to bedload transport depends on  
723 several parameters. The variation of the impulse frequency, the pulse length, beam focusing or associated internal  
724 signal processing (Broadband or Narrowband) can lead to different estimation of the apparent bedload velocity for  
725 the same sediment transport conditions (Conevski et al., 2020a). These parameters vary from a device to another  
726 (RDI/Sontek; Conevski et al., 2020b). As the aDcp pulse sample a volume of the riverbed (Rennie et al., 2002)  
727 which can lead to a biased estimation of  $V_a$ : *i*) an underestimation in case of large roughness of the riverbed with  
728 most of the reflected pulse is scattered by the immobile particles below the active layer (Conevski et al., 2019); *ii*)  
729 an overestimation in case of high concentration of the bedload layer (Rennie et al., 2017) or sand particles became  
730 in suspension near to the riverbed (water bias, Rennie et Millar, 2004). Even if a general trend seems to be  
731 highlighted by the river comparison (figure 3a) with an increasing bedload rate as grain size increases for a constant  
732  $V_a$ , the relationship between grain size and  $V_a$  cannot be easily determined in response to all variables mentioned  
733 above. One explanation of this trend could be that suspended sands could contribute to the bottom tracking signal

Supprimé: few time

Supprimé: an

Supprimé: in

Supprimé: very

Supprimé: 1

Mis en forme : Police :Italique

Supprimé: 2

Mis en forme : Police :Italique

Supprimé: described

741 without being caught by the sampler (Rennie et al., 2017). Moreover, the accuracy of the measurement on a single  
742 cross section depends on the water depth heterogeneity that in turn influences the aDcp footprint and makes the  
743 aDcp method location sensitive when bedforms are present (Fig. 9b). Estimation of bedload rates using empirical  
744 equations is limited by the number of variables that are difficult to measure in the field (e.g. thickness and  
745 concentration of active layer, Kostaschuck et al., 2005; Villard et al., 2005; Holmes, 2010; Latosinski et al., 2017;  
746 Conevski et al., 2018). The results shown in Fig. 4a suggest that Eq. (4) estimates sampler bedload rates if the  
747 projected bedload velocity is used. This kinematic model does not account for the thickness or the sediment  
748 concentration of the bedload layer and assumes that bedload transport never exceeds the size of a single particle  
749 assessed as uniform in terms of grain size (Rennie et al., 2002). These assumptions seems not appropriated for a  
750 sandy-gravel bed river. The active layer thickness should increase as suspended bed material load increases.  
751 Nevertheless, results are in agreement with BTMA bedload rates (Figure 4a). This can be explained by an  
752 underestimation of the apparent bedload velocity when it is projected along flow direction. On the other hand, Van  
753 Rijn (1984) defined the bedload layer thickness equal to the saltation height. The computed values of bedload layer  
754 thickness are coherent with other estimations performed on comparable rivers (Conevski et al., 2020a). The Eq.  
755 (5) better estimates sampler bedload rates using the raw bedload velocity (Figure 4b). If we consider that  $c_b$  and  $c_s$   
756 are well estimated by van Rijn equations (Eqs. 6 and 7), these results confirm that the projection of the apparent  
757 bedload velocity decreases the bedload velocity magnitude when the bedload direction differs from flow direction  
758 (e.g. bed slope effects). The influence of bedload velocity projection appears to be important when bedload are  
759 computed using kinematic models. Nevertheless, the calibration curve seems to be in agreement with other studies.  
760 Although, the application domain of Eq. (4) does not correspond to the conditions in the Loire River, the decrease  
761 of projected  $V_a$  seems to compensate the overestimation of bedload rates when the raw apparent bedload velocity  
762 is used. This is the opposite for Eq. (5) that accounts for bedload layer thickness and sediment concentration. In  
763 this case, the projection of  $V_a$  leads to underestimate bedload rates. Further works need to be done to improve the  
764 post-processing of  $V_a$  by recently published filtering procedures (Conevski et al., 2019 and 2020a) and to estimate  
765 its effect on calibration curve and kinematic models.  
766 Contrarily to the aDcp, the DTM allows the investigation of the "event active layer" (Church and Haschenburger,  
767 2017). The DTM is not a punctual measurement of bedload. Consequently, in presence of macroforms such as  
768 bars, it is difficult to compare with BTMA samples because it takes into account dunes that are not necessarily  
769 present at the BTMA sampling point (typically downstream a bar lee side). To some extent, the DTM and BTMA  
770 methods integrate bedload longitudinally at different scales. The presence of a local disturbance (or migrating  
771 bedform at low celerity) will affect the measurement. The determination of dune celerity by post-processing is time-  
772 consuming compared with the determination of dune morphology and the existing open access post-processing  
773 tools. In order to determine bedload rates with empirical equations, this method needs a calibration coefficient that  
774 is difficult to measure in field studies (Ten Brinke et al., 1999; Wilbers, 2004). Moreover, physical samplers sample

**Supprimé:** the equation  
**Supprimé:** n't  
**Supprimé:** take into  
**Supprimé:** made  
**Supprimé:** equation  
**Supprimé:** established  
**Supprimé:** line  
**Supprimé:** equation  
**Supprimé:** takes into  
**Supprimé:** Several laboratory studies have been carried out (Ramooz and Rennie, 2010; Conevski 2019) and rivers instrumented with aDcp to determine bedload rates (Rennie et al., 2002; Rennie and Millar, 2004; Gaeuman and Jacobson, 2006; Gaeuman and Pittman, 2010; Brasington et al., 2011). This method remains site-specific and there is no general agreement between bedload rates and apparent velocity (Rennie and Villard, 2004). The response of aDcp to bedload transport depends on the frequency of the device used and grain size (Gaeuman and Rennie, 2006) with a strong influence of near-bed suspended sediments in sandy environment (Rennie et al., 2002). Moreover, the accuracy of the measurement on a single cross section depends on the water depth heterogeneity that influences the bottom track sampling area of beams and make the aDcp method location sensitive when bedforms are present (Fig. 8b). When negative values of apparent bedload velocity are measured, the value is considered as null and interpolated over a width that is probably wider than the effective width where bedload transport is null. In consequence, total bedload transport rates estimated with Eq. (14) lead to an underestimation of BTMA bedload transport rates, especially for low water discharge (Fig. 6b). Estimation of bedload rates using empirical equations is limited by the number of variables that are difficult to measure in the field (e.g. thickness and concentration of active layer, Conevski et al., 2018; Holmes, 2010; Kostaschuck et al., 2005; Latosinski et al., 2017; Villard et al., 2005). Results of 3b suggest that the apparent bedload velocity measured by aDcp is the velocity of a sediment layer of about  $1D_{50}$  thick, defined by Church and Haschenburger (2017) as the "dynamic active layer". This result is in agreement with observations made during this study with video recorders for low flow conditions but it can be criticized for high flow conditions in a sandy-gravel bed river. The active layer thickness should increase with discharge as more particles are transported as suspension. Van Rijn (1984) defined the bedload layer thickness equal to the saltation height. Bedload transport rates calculated using Eq. (5) and Eq. (6) were overestimated in comparison of those measured with BTMA. If we consider that the thickness of active layer is underestimated for these hydraulic conditions in the Eq. (4) (equal to  $D_{50}$ ), this suggests that the apparent bedload velocity could be overestimated by aDcp when sediments are in suspension near the bed (water bias) and the aDcp frequency is too high (M9, 3 MHz). In this study, the high aDcp frequency seems to compensate the underestimation of bedload layer thickness in the Eq. (4) by measuring higher apparent velocity of particles in saltation/suspension. In the case of the use of Eq. (5) and Eq. (6), the aDcp frequency ...

882 the dynamical active layer, thus more comparable to the hydrophones and aDcps. Nevertheless, DTM remains an  
883 accurate method to estimate bedload transport in the Loire River (Fig. 6b) where dunes are present and high  
884 enough (over the mean annual discharge).

885 As suggested by previous authors, both aDcp (Kenney, 2006) and hydrophone (Bedeus and Ivicsics, 1963) allow  
886 a reliable representation of bedload fluxes on a cross section through the regressions with bedload rates obtained  
887 using samplers. Fig. 9a and Fig. 9b highlight the benefits of the use of acoustics devices for the determination of  
888 bedload transport rates in a large sandy gravel-bed rivers. In the present study, the time needed in the field to  
889 complete the BTMA, DTM, aDcp and hydrophone methods (respectively the red, yellow, blue and black lines of  
890 Fig. 9b), are about 1 day, 4 hours, 1.5 hours and 45 minutes, respectively. These times were estimated including  
891 the time needed to position and anchor the boat at each sampling point. This underlines the high potential of  
892 hydrophones to quantify bedload in large rivers with high spatial variability of sediment transport and map bedload  
893 sediment fluxes at a large scale as proposed by Williams et al. (2015) using the aDcp. Moreover, all indirect  
894 methods tested here seem to be able to quantify total bedload transport as efficient as the direct method (Fig. 6b)  
895 but special care should be taken with local estimation of bedload rates (Fig. 9a and Fig. 9b).

896 Finally, regarding the correlation of aDcp and hydrophone with BTMA (Fig. 3a and Fig. 5b), we can raise the  
897 question of the reference method. Indeed, the regression between aDcp and hydrophone is more significant  
898 ( $R^2=0.76$ ) and it could be the quality and the accuracy of BTMA sampling that reduce the quality of indirect  
899 measurement regressions.

## 900 5.2. Hydrophone and aDcp sensitivity to bedform observations

901 Passive (hydrophone) and active (aDcp) acoustic devices are rarely used to analyse of bedload transport rates  
902 associated with bedforms in relatively large lowland rivers. Several studies mention differences in apparent bedload  
903 velocity according to the location on bedforms (Rennie and Millar, 2004; Villard and Church, 2005; Gaeuman and  
904 Jacobson, 2006; Holmes, 2010; Latosinski et al., 2017). These authors have shown that apparent bedload velocity  
905 increases from trough to crest of the dune and confirmed previous observations made with samplers (Kostachuck  
906 and Villard, 1996; Carling et al., 2000). These observations were made on large dunes that migrate too slowly to  
907 allow a continuous measurement along bedforms. Our study complements these observations by providing a fixed  
908 and continuous measurement of apparent bedload velocity and providing bedload transport rates estimation based  
909 on a calibration curve. The mean time between two subsequent crests (1 hour) shows that even for small bedforms  
910 ( $H_D=0.05$  to  $0.2$  m, Fig. 10a and Fig. 10b), the aDcp location significantly influences the bedload rates calculated  
911 over a dune field ( $0.03$  to  $0.08$   $m \cdot s^{-1}$  of difference between crest and trough). This suggests that care should be  
912 taken using this method on river beds where large dunes are present but also when small dunes are migrating.

913 According to Rennie and Millar (2004), the sampling area diameter increases with the water depth and is  
914 approximately equal to flow depth. Our protocol minimizes the water depth by submerging the aDcp and therefore

Supprimé: d

Supprimé: red, yellow, blue and black lines of Fig. 8b (BTMA, DTM, aDcp and hydrophone methods, respectively)

Supprimé: to

Supprimé: for analysis

Supprimé: completes

Supprimé: offering

Supprimé: flow

Supprimé: more or less

Supprimé: flow

925 minimizes the beams sampling diameter, hence, minimizes the probability to sample stoss or lee sides of the same  
926 dune simultaneously.

927 In our study context, the acoustic power recorded by the hydrophone was not affected by the distance between the  
928 hydrophone and the river bed. To our knowledge, there are no references mentioning investigations on bedload  
929 transport rates associated with bedforms using a hydrophone. At a large time step (mean aDcp and hydrophone  
930 samples), the apparent bedload velocity and the acoustic power did not follow the observed trend of mean bedform  
931 characteristics derived from DTM measurement (dune celerity and dune height). This could be explained by the  
932 difference of spatial scales between DTM and other methods. For a smaller time step, our results showed that  
933 acoustic power is able to describe the influence of bars on bedload sediment transport (Fig. 11a). Moreover, as for  
934 the aDcp, the hydrophone also detects the theoretical pattern of bedload transport rates associated with bedform  
935 migration. As shown by Reesink et al. (2014), the lee effect generated by bar fronts influences the development of  
936 dunes downstream. Specifically, the hydrophone is able to record the decrease of the acoustic power immediately  
937 downstream the bar front and its progressive increase downstream (traduced by the development of dunes at about  
938 11h06. Fig. 11a). In the present study, dunes smaller than 0.4 m (Fig. 11a) were not high enough to allow the  
939 observation of changes in the acoustic power along the bedform stoss sides. On the contrary, for higher dunes ( $H_D$   
940 = 1 m, Fig. 11b) the bedload generated noise can be well recorded by the hydrophone. A hydrophone senses every  
941 noises that are propagating in the water column. Therefore, the hydrophone can record noises that is far away from  
942 its location. Noises are more and more attenuated with increasing distance (Geay et al., 2019). Particularly, when  
943 there is few bedload noise, close to the hydrophone, the hydrophone can sense the bedload noise, that are  
944 generated far away. This behaviour could explain why the hydrophone tends to overestimate bedload fluxes when  
945 bedload fluxes are weak especially immediately downstream a bar front (Fig. 9b).  
946 Hydrophone lower detection limit was not reached during our study whereas the dispersion of bedload rates  
947 measured with samplers for low apparent bedload velocity suggests that the lower detection limit of the apparent  
948 bedload velocity by the aDcp seems to be about 1 cm.s<sup>-1</sup> (Rennie et al., 2017). This lower detection limit of the  
949 apparent bedload velocity should be reduced to the bottom track uncertainty by using our protocol with a  
950 submerged and fixed aDcp device.

## 951 6. Conclusions

952 In this work, direct (BTMA samplers) with active (aDcp and DTM) and passive (hydrophone) acoustic  
953 measurements of bedload transport rates were compared in a large, sandy-gravel bed river characterized by the  
954 presence of bars and superimposed dunes. Calibration curves between apparent bedload velocity measured using  
955 aDcp and bedload rates measured using BTMA samplers were established but remain site-specific and dependent  
956 to grain size. DTM seemed to be inappropriate where macroforms are present, as it influences the location and the

Supprimé: finer

Supprimé: Moreover, as for the aDcp, the hydrophone also detects the theoretical pattern of bedload transport rates associated with dune migration. As shown by Reesink et al. (2014), the presence of bars influences the development of dunes downstream and the distance between bar crest and dune initiation point increases with flow velocity. Specifically, the hydrophone is able to record an increasing acoustic power assumed to be associated with the increasing dune height downstream of the bedform initiation point (about 11h06, Fig. 10a).

Supprimé: Conversely

Supprimé: sense

Supprimé: are

Supprimé: s

Supprimé: s

Supprimé: isokinetic

Supprimé: strongly correlated

975 size of superimposed mesoforms. The calculation of bedload rates with empirical formulas is sensitive to bedload  
976 discharge coefficient for DTM and to thickness and concentration of active layer for aDcp. These parameters remain  
977 difficult to measure in the field. Results presented in this study highlight the potential of the hydrophone for the  
978 quantification and mapping of bedload transport rates in relatively large river channels where migrating bedforms  
979 are present while it was mainly used until today to monitor bedload transport rates in gravel-bed rivers. This study  
980 consolidates a recent study (Geay et al., 2020) by extending a general calibration curve to large sandy-gravel bed  
981 rivers. The hydrophone global calibration curve allows a good representation of the bedload fluxes evolution  
982 through a cross section. The method is more affordable to implement and more efficient than the reference method.  
983 This might allow mapping bedload transport rates by interpolating acoustic power along several cross sections  
984 performed on a large sandy gravel bed river. Moreover, acoustic devices (aDcp and hydrophone) are able to  
985 capture the evolution of bedload signal along bedforms stoss and lee sides with some limitation of bedform size for  
986 the hydrophone and signal noise for the aDcp. Regarding results of the comparison between bedload velocity and  
987 acoustic power, the association of aDcp and hydrophone could be an efficient way to control the quality of both  
988 devices. However, additional measurements and post-processing tasks are needed (Conevski et al., 2019) to  
989 explore the quality of the regression in other river environments (different grain sizes, river-bed slope or propagation  
990 effect).  
991

**Supprimé:** always

**Supprimé:** The use of the hydrophone to monitor bedload transport rates is, for the moment, mainly limited to gravel-bed rivers.

**Supprimé:** this technique

**Supprimé:** previous

**Supprimé:** cheaper

**Supprimé:** catch

**Supprimé:** need to be done

**Supprimé:** Finally, the lack of post-processing open access tools for these surrogate technologies slow the development and use of these devices to bedload rates determination.

1004 **Appendices**

1005 Appendix A: Hydrophone dataset

1006

Date	Number of Hydrophone Drifts	average drift duration (s)	mean acoustic power (Pa <sup>2</sup> )
08/02/2018	24	60	2.17E+13
17/05/2018	24	80	1.46E+12
15/04/2019	11	37	1.66E+12
16/04/2019	11	42	2.25E+12
17/04/2019	11	28	1.42E+12
18/04/2019	11	30	2.35E+12
27/05/2019	8	42	5.07E+11
29/05/2019	9	36	2.00E+12
09/12/2019	22	29	6.67E+12
10/12/2019	21	22	7.69E+12
11/12/2019	22	27	8.84E+12
12/12/2019	13	27	8.97E+12
19/12/2019	22	25	2.41E+13
18/05/2020	8	50	4.53E+12
19/05/2020	8	30	3.82E+12
20/05/2020	17	36	3.07E+12

1007

1008

1009 Appendix B: ADcp dataset  
1010

Date	Number of aDcp sampling points	aDcp frequency (kHz)	aDcp type	<u>Pulse</u> <u>type</u> *1 *2	Average aDcp sampling duration (s)	mean Va (m.s <sup>-1</sup> )	mean water depth (m)	mean flow velocity (m.s <sup>-1</sup> )
27/03/2017	4	1200	RG	<u>BB</u>	3909	0.013	2.0	0.7
28/03/2017	4	1200	RG	<u>BB</u>	3279	0.015	2.1	0.7
29/03/2017	4	1200	RG	<u>BB</u>	3276	0.011	2.2	0.7
30/03/2017	4	1200	RG	<u>BB</u>	1707	0.009	2.1	0.8
15/05/2017	3	1200	RG	<u>BB</u>	3018	0.002	1.3	0.8
16/05/2017	2	1200	RG	<u>BB</u>	2315	0.010	1.0	0.8
17/05/2017	3	1200	RG	<u>BB</u>	2618	0.003	1.4	0.8
18/05/2017	3	1200	RG	<u>BB</u>	2467	0.002	1.6	0.8
04/12/2017	3	1200	RG	<u>BB</u>	2647	0.000	1.2	0.7
05/12/2017	3	1200	RG	<u>BB</u>	2657	0.008	1.2	0.6
06/12/2017	3	1200	RG	<u>BB</u>	2246	0.000	1.2	0.7
07/12/2017	3	1200	RG	<u>BB</u>	2588	0.002	1.3	0.7
08/12/2017	3	1200	RG	<u>BB</u>	3400	0.003	1.2	0.6
15/01/2018	3	1200	RG	<u>BB</u>	3256	0.084	3.2	1.1
16/01/2018	3	1200	RG	<u>BB</u>	1800	0.058	2.9	1.0
17/01/2018	4	1200	RG	<u>BB</u>	3185	0.041	2.7	1.0
18/01/2018	4	1200	RG	<u>BB</u>	3656	0.055	2.8	1.0
19/01/2018	3	1200	RG	<u>BB</u>	2029	0.075	2.7	1.1
30/01/2018	3	1200	RG	<u>BB</u>	2138	0.051	3.9	1.1
31/01/2018	3	1200	RG	<u>BB</u>	2056	0.070	3.7	1.1
08/02/2018	4	3000	M9	<u>BB</u>	1136	0.038	2.8	0.9
14/05/2018	4	3000	M9	<u>BB</u>	2130	0.002	1.2	0.6
15/05/2018	4	variable	M9	<u>HD</u>	1133	0.011	1.5	0.6
16/05/2018	3	variable	M9	<u>HD</u>	948	0.002	1.4	0.7
17/05/2018	3	1200	RG	<u>BB</u>	1346	0.003	1.7	0.7
15/04/2019	3	variable	M9	<u>HD</u>	2601	0.009	1.2	0.8
16/04/2019	3	3000	M9	<u>NB</u>	1687	0.006	1.1	0.7
17/04/2019	3	variable	M9	<u>HD</u>	1152	0.010	1.0	0.7
18/04/2019	3	variable	M9	<u>HD</u>	3580	0.008	0.9	0.7

27/05/2019	1	3000	M9	<a href="#">NB</a>	10949	0.003	0.9	0.8
29/05/2019	1	3000	M9	<a href="#">NB</a>	11539	0.029	0.9	0.7
09/12/2019	2	3000	M9	<a href="#">NB</a>	1753	0.023	1.7	0.8
10/12/2019	3	3000	M9	<a href="#">NB</a>	1160	0.018	2.1	0.8
11/12/2019	3	3000	M9	<a href="#">NB</a>	1288	0.027	1.6	0.9
12/12/2019	2	3000	M9	<a href="#">NB</a>	1349	0.032	2.1	0.8
19/12/2019	5	3000	M9	<a href="#">NB</a>	1221	0.056	3.0	1.1
19/05/2020	2	3000	M9	<a href="#">NB</a>	7318	0.014	1.0	0.7
20/05/2020	4	3000	M9	<a href="#">NB</a>	2988	0.004	1.6	0.7

1011 [\\*1: RG = aDcp Rio Grande RDI; M9 = aDcp M9 Sontek](#)

1012 [\\*2 BB = Broadband \(coherent Pulse\); NB = Narrowband \(incoherent pulse\); HD = Smartpulse HD](#)

1013



1014 Appendix C: BTMA dataset  
1015

Date	Discharge (m <sup>3</sup> .s <sup>-1</sup> )	Measurements type	Number of BTMA sampling points	Number of BTMA samples	Mean unit bedload rate (g.s <sup>-1</sup> .m <sup>-1</sup> )	D50 (mm)	D90 (mm)
28/11/2016	1420	BTMA & DTM	3	50	38.1	0.8	3.0
29/11/2016	1460	BTMA & DTM	4	79	31.5	0.9	3.5
30/11/2016	1300	BTMA & DTM	4	80	33.2	0.8	2.9
01/12/2016	1100	BTMA & DTM	4	79	32.2	0.8	2.6
27/03/2017	687	BTMA. aDcp & DTM	4	80	25.3	0.7	2.9
28/03/2017	752	BTMA. aDcp & DTM	4	80	28.5	0.8	3.0
29/03/2017	827	BTMA. aDcp & DTM	4	57	29.0	0.8	3.8
30/03/2017	812	BTMA. aDcp & DTM	4	80	19.3	0.8	3.8
15/05/2017	346	BTMA. aDcp & DTM	3	60	6.3	0.9	4.8
16/05/2017	354	BTMA. aDcp & DTM	3	60	13.5	0.8	5.0
17/05/2017	401	BTMA. aDcp & DTM	3	55	9.0	0.9	4.7
18/05/2017	447	BTMA. aDcp & DTM	3	60	1.9	1.2	7.0
04/12/2017	243	BTMA & aDcp	3	60	1.8	1.1	7.4
05/12/2017	241	BTMA. aDcp & DTM	3	60	3.7	1.0	8.6
06/12/2017	243	BTMA. aDcp & DTM	3	60	6.6	1.2	6.7
07/12/2017	246	BTMA. aDcp & DTM	3	60	5.1	1.2	5.1
08/12/2017	226	BTMA. aDcp & DTM	3	60	5.0	1.6	7.9
15/01/2018	1740	BTMA. aDcp & DTM	3	60	61.4	1.0	2.9
16/01/2018	1550	BTMA. aDcp & DTM	3	60	89.4	0.9	2.8
17/01/2018	1460	BTMA. aDcp & DTM	4	80	53.2	0.8	3.0
18/01/2018	1540	BTMA. aDcp & DTM	4	80	97.7	1.0	3.3
19/01/2018	1510	BTMA. aDcp & DTM	3	60	55.6	0.8	2.6
30/01/2018	2410	BTMA. aDcp & DTM	3	60	68.6	0.8	2.3
31/01/2018	2290	BTMA. aDcp & DTM	3	59	55.8	0.8	2.2
08/02/2018	1550	BTMA. aDcp. DTM. Hydrophone	4	69	63.4	0.8	2.5
14/05/2018	443	BTMA. aDcp & DTM	4	79	2.2	0.9	2.7
15/05/2018	449	BTMA & aDcp	4	79	2.5	1.1	3.2

16/05/2018	547	BTMA. aDcp & DTM	3	60	6.6	1.2	4.4
17/05/2018	604	BTMA. aDcp. DTM. Hydrophone	3	60	7.2	1.2	4.4
15/04/2019	253	BTMA. aDcp & Hydrophone	3	60	22.1	0.9	3.3
16/04/2019	243	BTMA. aDcp & Hydrophone	3	60	22.1	1.1	5.1
17/04/2019	240	BTMA. aDcp & Hydrophone	3	60	24.9	1.2	3.7
18/04/2019	238	BTMA. aDcp & Hydrophone	3	58	16.4	1.0	5.3
27/05/2019	225	BTMA. aDcp. DTM. Hydrophone	1	26	34.6	1.0	4.8
29/05/2019	210	BTMA. aDcp. DTM. Hydrophone	1	28	22.0	1.1	3.3
09/12/2019	944	BTMA. aDcp. DTM. Hydrophone	2	40	29.1	0.7	2.5
10/12/2019	898	BTMA. aDcp. DTM. Hydrophone	3	60	20.1	0.6	2.5
11/12/2019	923	BTMA. aDcp. DTM. Hydrophone	3	45	34.9	0.8	2.4
12/12/2019	925	BTMA. aDcp. DTM. Hydrophone	2	37	26.4	0.7	2.7
19/12/2019	2050	BTMA. aDcp. DTM. Hydrophone	5	50	58.8	0.9	3.4
18/05/2020	514	BTMA & Hydrophone	1	57	19.7	0.9	2.8
19/05/2020	500	BTMA. aDcp & Hydrophone	2	79	30.9	1.0	2.6
20/05/2020	470	BTMA. aDcp & Hydrophone	4	40	14.5	-	-

1016  
1017

1018 Appendix D: DTM dataset  
 1019

Date	Number of DTM profiles	average interval time DTM (min)	Number of dunes	Mean H <sub>D</sub> (m)	Mean L <sub>D</sub> (m)	Mean C <sub>D</sub> (m.d <sup>-1</sup> )
28/11/2016	2	18	65	0.19	2.88	43.0
29/11/2016	3	20	168	0.22	3.69	34.8
30/11/2016	3	18	121	0.24	4.16	37.6
01/12/2016	3	19	104	0.25	4.69	37.6
27/03/2017	3	38	132	0.13	3.13	28.3
28/03/2017	3	44	97	0.13	2.96	24.2
29/03/2017	3	43	117	0.14	3.25	25.7
30/03/2017	3	39	138	0.14	3.42	28.0
15/05/2017	3	65	20	0.04	2.17	18.1
16/05/2017	3	42	11	0.05	2.02	26.7
17/05/2017	3	38	18	0.05	2.01	28.0
18/05/2017	3	28	34	0.08	1.95	30.9
05/12/2017	1	73	48	0.13	2.90	17.9
06/12/2017	1	98	68	0.16	3.44	14.9
07/12/2017	1	72	63	0.17	3.62	17.3
08/12/2017	1	66	69	0.19	3.95	14.8
15/01/2018	6	23	228	0.32	6.66	38.1
16/01/2018	2	28	46	0.24	3.58	47.6
17/01/2018	3	32	52	0.25	4.36	34.9
18/01/2018	3	55	120	0.28	5.33	28.0
19/01/2018	3	31	110	0.26	4.95	31.4
30/01/2018	3	25	103	0.32	5.75	45.3
31/01/2018	4	22	83	0.28	5.02	45.4
08/02/2018	3	60	59	0.26	4.67	28.2
14/05/2018	6	35	58	0.06	2.92	20.8
16/05/2018	4	38	60	0.05	1.96	18.8
17/05/2018	6	34	81	0.05	1.98	22.3
27/05/2019	1	29	3	0.03	1.40	62.7
29/05/2019	1	26	7	0.03	1.28	30.7

09/12/2019	6	49	121	0.22	3.10	28.1
10/12/2019	6	42	227	0.17	3.60	33.2
11/12/2019	6	49	254	0.16	3.46	33.1
12/12/2019	6	50	297	0.18	3.82	35.9
19/12/2019	3	44	79	0.28	4.34	42.1

1020

1021

1022 **Video supplement**

1023 [Videos of BTMA sampling were added in supplement of this manuscript to appreciate the variability of bedload in](#)  
1024 [the Loire River.](#)  
1025 <https://doi.org/10.5446/51563>  
1026 <https://doi.org/10.5446/51562>  
1027 <https://doi.org/10.5446/51561>  
1028 <https://doi.org/10.5446/51560>

1029 **Author contribution**

1030 J. Le Guern prepared the manuscript with contributions from all co-authors. [J. le Guern](#), T. Geay, A. Hauet, S.  
1031 Zanker, S. Rodrigues [elaborated](#) the experimental protocol. T. Geay developed the hydrophone signal processing  
1032 tools. A. Duperray P. Jugé, L. Vervynck, A. Hauet, S. Zanker, T. Geay, S. Rodrigues and J. Le Guern [conducted](#)  
1033 [the field surveys](#). A. Duperray P. Jugé, and L. Vervynck [performed](#) the bathymetry post-processing. S. Rodrigues,  
1034 and P. Tassi supervised this study. [N. Claude helped in the analysis of BTMA and aDcp measurements.](#)

Supprimé: helped to

Supprimé: took part in surveys

Supprimé: made

Supprimé: ,

Supprimé: N. Claude

1035 **Competing interests**

1036 The authors declare that they have no conflict of interest.

1037 **Acknowledgement**

1038 This study is a part of the Ph.D. thesis of the first author funded by the POI FEDER Loire (Convention no. 2017-  
1039 EX002207) and Agence de l'Eau Loire Bretagne (decision no.2017C005), conducted in the frame of the Masterplan  
1040 Plan Loire Grandeur Nature. We thank EDF DTG and [ARD](#) Intelligence des Patrimoines (Phase 2) for lending us  
1041 acquisition equipment. Exagone Company is acknowledged for providing us data from Teria network, Voie  
1042 Navigable de France (VNF) for their logistical support during field [surveys](#), and Polytech Tours. J.-P. Bakyono, P.  
1043 Berault, T. Bulteau, B. Deleplancouille, Y. Guerez, T. Handfus, I. Pene and C. Wintenberger, are acknowledged  
1044 for their help during field investigations and grain size analyses. We are grateful to T. Geay and J. Hugueny for the  
1045 hydrophone treatment and aDcp data post-processing tools, respectively. The authors wish [to thank Pr. K. M.](#)  
1046 [Wantzen for checking the English quality](#) of the manuscript.

Supprimé: ANR

Supprimé: campaigns

Supprimé: the English translation

1055 **References**

- 1056 Batalla, R. J.: Evaluation bed-material transport equations using field measurements in a sandy gravel-bed stream,  
1057 Arbúcies River, NE Spain, *Earth Surf. Process. Landforms*, 22 (2), 121-130, [https://doi.org/10.1002/\(SICI\)1096-9837\(199702\)22:2<121::AID-ESP671>3.0.CO;2-7](https://doi.org/10.1002/(SICI)1096-9837(199702)22:2<121::AID-ESP671>3.0.CO;2-7), 1997.
- 1058 [Banhold, K., Schüttrumpf, H., Hillebrand, G. and Frings, R.: Underestimation of sand loads during bed-load measurements- a laboratory examination, in: Proceedings of the international conference on Fluvial Hydraulics \(River Flow 2016\). 11-14 July 2016, Saint Louis, USA, 2406 pp., 2016.](#)
- 1059 [Barton, J., Slingerland, R. R. L., Pittman, S., and Gabrielson, T. B.: Monitoring coarse bedload transport with passive acoustic instrumentation: A field study, US Geol. Surv. Sci. Investig. Rep., 38–51, 2010.](#)
- 1060 [Bedeus, K., and Ivicsics, L.: Observation of the noise of bed load, Gen. Assem. Comm. Hydrom. Int. Assoc. Hydrol. Sci. Berkeley, CA, USA, 19–31, 1963.](#)
- 1061 [Bertoldi, W., Ashmore, P., and Tubino, M.: A method for estimating the mean bed load flux in braided rivers, Geomorphology, 103, 330-340, https://doi.org/10.1016/j.geomorph.2008.06.014, 2009.](#)
- 1062 [Best, J. L.: Sediment transport and bed morphology at river channel confluences, Sedimentology, 35, 481-498, https://doi.org/10.1111/j.1365-3091.1988.tb00999.x, 1988.](#)
- 1063 [Blanpain, O., Demoulin, X., Waeles, B., Ravilly, M., Garlan, T., and Guyomard, P.: Passive acoustic measurement of bedload discharge features on a sandy seafloor, in: Proceedings of Seabed and Sediment Acoustics Volume 37 Part 1, Bath, United Kingdom, 7-9 september 2015.](#)
- 1064 [Blott, S. J., and Pye, K.: GRADISTAT: A grain size distribution and statistics package for the analysis of unconsolidated sediments, Earth Surf. Process. Landforms, 26 \(11\), 1237-1248, https://doi.org/10.1002/esp.261, 2001.](#)
- 1065 [Boiten, W.: Hydrometry, IHE Delft Lecture Note Series, A.A. Balkema Publishers, Netherland, 256 pp, https://doi.org/10.1201/9780203971093, 2003.](#)
- 1066 [Brasington, J., Rennie, C. D., Vericat, D., Williams, R., Goodsell, B., Hicks, M., and Batalla, R.: Monitoring braided river morphodynamics with an acoustic Doppler current profiler, in: Proceedings of the 34th World Congress of the International Association for Hydro-Environment Research and Engineering: 33rd Hydrology and Water Resources Symposium and 10th Conference on Hydraulics in Water Engineering, Brisbane, 3396-3403, 2011.](#)
- 1067 [Carling, P. A., Williams, J. J., Götz, E., and Kelsey, A. D.: The morphodynamics of fluvial sand dunes in the River Rhine, near Mainz, Germany. II. Hydrodynamics and sediment transport, Sedimentology, 47, 253-278, https://doi.org/10.1046/j.1365-3091.2000.00291.x, 2000.](#)
- 1068 [Church, M., and Haschenburger, J. K.: What is the “active layer”?, Water Resour. Res., 53 \(1\), 5-10, https://doi.org/10.1002/2016WR019675, 2017.](#)

1087 Claude, N., Rodrigues, S., Bustillo, V., Bréhéret, J. G., Macaire, J. J., and Jugé, P.: Estimating bedload transport  
1088 in a large sand-gravel bed river from direct sampling, dune tracking and empirical formulas, *Geomorphology*, 179,  
1089 40-57, <https://doi.org/10.1016/j.geomorph.2012.07.030>, 2012.

1090 Claude, N., Rodrigues, S., Bustillo, V., Bréhéret, J. G., Tassi, P., and Jugé, P.: Interactions between flow structure  
1091 and morphodynamic of bars in a channel expansion/contraction, Loire River, France, *Water Resour. Res.*, 50,  
1092 <https://doi.org/10.1002/2013WR015182>, 2014.

1093 Conevski, S.: Bedload Monitoring by means of Hydro-Acoustic Techniques, Ph.D. thesis, Norwegian University of  
1094 Science and Technology, Norway, 200 pp., 2018.

1095 [Conevski, S., Guerrero, M., Ruther N., and Rennie, C. D.: Laboratory investigation of apparent bedload velocity  
1096 measured by ADCPs under different transport conditions, \*J. Hydraul. Eng.\*, 145 \(11\),  
1097 \[https://doi.org/10.1061/\\(ASCE\\)HY.1943-7900.0001632\]\(https://doi.org/10.1061/\(ASCE\)HY.1943-7900.0001632\), 2019.](https://doi.org/10.1061/(ASCE)HY.1943-7900.0001632)

1098 [Conevski, S., Guerrero, M., Winterscheid, A., Rennie, C. D., and Ruther N.: Acoustic sampling effects on bedload  
1099 quantification using acoustic Doppler current profilers, \*Journal of Hydraulic Research\*,  
1100 <https://doi.org/10.1080/00221686.2019.1703047>, 2020a.](https://doi.org/10.1080/00221686.2019.1703047)

1101 [Conevski, S., Guerrero, M., Rennie, C. D., and Ruther, N.: Towards an evaluation of bedload transport  
1102 characteristics by using Doppler and backscatter outputs from ADCPs, \*Journal of Hydraulic Research\*,  
1103 <https://doi.org/10.1080/00221686.2020.1818311>, 2020b.](https://doi.org/10.1080/00221686.2020.1818311)

1104 Cordier, F., Tassi, P., Claude, N., Crosato, A., Rodrigues, S., and Pham Van Bang, D.: Bar pattern and sediment  
1105 sorting in channel contraction/expansion area: Application to the Loire River at Bréhémont (France), *Advances in  
1106 Water Resources*, 140, <https://doi.org/10.1016/j.advwatres.2020.103580>, 2020.

1107 [de Vries, M.: Information on the Arnhem Sampler \(BTMA\), Internal Report n°3-79, Delft University of Technology,  
1108 Department of Civil Engineering, Fluid Mechanics Group, 1979.](https://doi.org/10.1016/j.advwatres.2020.103580)

1109 Eijkelkamp: Operating instructions: Bedload Transport Meter Arnhem, Giesbeek, Netherland, 8 pp., 2003.

1110 Engel, P., and Lau, Y. L.: Computation of Bed Load Using Bathymetric Data, *Journal of the Hydraulics Division*,  
1111 106 (3), 369-380, 1980.

1112 Folk, R. L., and Ward, W. C.: Brazos River bar (Texas); a study in the significance of grain size parameters, *Journal  
1113 of Sedimentary Research*, 27 (1), 3-26, <https://doi.org/10.1306/74D70646-2B21-11D7-8648000102C1865D>, 1957.

1114 [Frings, R. M., and Vollmer, S.: Guidelines for sampling bed-load transport with minimum uncertainty,  
1115 \*Sedimentology\*, 64 \(6\), 1630-1645, <https://doi.org/10.1111/sed.12366>, 2017.](https://doi.org/10.1111/sed.12366)

1116 [Frings, R. M., Gehres, N., Promny, M., Middelkoop, H., Schüttrumpf, H., and Vollmer, S.: Today's sediment budget  
1117 of the Rhine River channel, focusing on the Upper Rhine Graben and Rhenish Massif, \*Geomorphology\*, 204, 573-  
1118 587, <https://doi.org/10.1016/j.geomorph.2013.08.035>, 2014.](https://doi.org/10.1016/j.geomorph.2013.08.035)

1119 Gaeuman, D., and Jacobson, R. B.: Acoustic bed velocity and bed load dynamics in a large sand bed river, *J.  
1120 Geophys. Res.*, 111, F02005, <https://doi.org/10.1029/2005JF000411>, 2006.

1121 Gaeuman, D., and Jacobson, R. B.: Field Assessment of Alternative Bed-Load Transport Estimators, *J. Hydraul.*  
1122 *Eng.*, 133 (12), 1319-1328, [https://doi.org/10.1061/\(ASCE\)0733-9429\(2007\)133:12\(1319\)](https://doi.org/10.1061/(ASCE)0733-9429(2007)133:12(1319)), 2007.

1123 Gaeuman, D., and Pittman, S.: Relative Contributions of Sand and Gravel Bedload Transport to Acoustic Doppler  
1124 Bed-Velocity Magnitudes in the Trinity River, California, U.S. Geological Survey Scientific Investigations Report,  
1125 2010-5091, 2010.

1126 [Gaweesh, M. T. K., and van Rijn, L. C.: Bed-load sampling in sand-bed rivers, \*J. Hydraul. Eng.\*, 120 \(12\), 1364-](https://doi.org/10.1061/(ASCE)0733-9429(1994)120:12(1364))  
1127 [1384, https://doi.org/10.1061/\(ASCE\)0733-9429\(1994\)120:12\(1364\)](https://doi.org/10.1061/(ASCE)0733-9429(1994)120:12(1364)), 1994.

1128 Geay, T., Belleudy, P., Gervaise, C., Habersack, H., Aigner, J., Kreisler, A., Seitz, H., and Laronne, J. B.: Passive  
1129 acoustic monitoring of bed load discharge in a large gravel bed river, *J. Geophys. Res.: Earth Surf.*, 122 (2),  
1130 <https://doi.org/10.1002/2016JF004112>, 2017.

1131 Geay, T., Michel, L., Zanker, S., and Rigby, J. R.: Acoustic wave propagation in rivers: an experimental study. *Earth*  
1132 *Surface Dynamics*, 7 (2), 537–548, <https://doi.org/10.5194/esurf-7-537-2019>, 2019.

1133 Geay, T., Zanker, S., Misset, C., and Recking, A.: Passive Acoustic Measurement of Bedload Transport: Toward  
1134 a Global Calibration Curve?, *J. Geophys. Res.: Earth Surf.*, 125 (8), <https://doi.org/10.1029/2019JF005242>, 2020.

1135 Gimbert, F., Fuller, B. M., Lamb, M. P., Tsai, V. C., and Johnson, J. P. L.: Particle transport mechanics and induced  
1136 seismic noise in steep flume experiments with accelerometer-embedded tracers, *Earth Surf. Process. Landforms*,  
1137 44, 219-241, <https://doi.org/10.1002/esp.4495>, 2019.

1138 Gray, J. R., Gartner, J. W., Barton, J. S., Gaskin, J., Pittman, S. A., and Rennie, C. D.: Surrogate Technologies for  
1139 Monitoring Bed-Load Transport in Rivers, *Sedimentology of Aqueous Systems*, 46-79,  
1140 <https://doi.org/10.1002/9781444317114.ch2>, 2010.

1141 Grill, G., Lehner, B., Thieme, M. et al.: Mapping the world's free-flowing rivers. *Nature* 569, 215–221,  
1142 <https://doi.org/10.1038/s41586-019-1111-9>, 2019.

1143 Hilldale, R. C., Goodwillier, B. T., Carpenter, W. O., and Chambers, J. P.: Measuring Coarse Bed Load Using  
1144 Hydrophones, Closeout report, Reclamation Managing Water in the West, 2014.

1145 Holmes, R. R. Jr.: Measurement of Bedload Transport in Sand-Bed Rivers: A Look at Two Indirect Sampling  
1146 Methods, U.S. Geological Survey Scientific Investigations Report, 2010-5091, 2010.

1147 Jackson, R. G.: Hierarchical attributes and a unifying model of bed forms composed of cohesionless material and  
1148 produced by shearing flow, *Geological Society of America Bulletin*, 86, 1523-1533, 1975.

1149 Jamieson, E. C., Rennie, C. D., Jacobson, R. B., and Townsend, R. D.: Evaluation of ADCP Apparent Bed Load  
1150 Velocity in a large Sand-Bed River: Moving versus Stationary Boat Conditions, *J. Hydraul. Eng.*, 137, 1064-1071,  
1151 [https://doi.org/10.1061/\(ASCE\)HY.1943-7900.0000373](https://doi.org/10.1061/(ASCE)HY.1943-7900.0000373), 2011.

1152 Kenney, T. A. (2006), Cross-sectional progression of apparent bedload velocities, in: Proceedings of the Eighth  
1153 Federal Interagency Sedimentation Conference (8<sup>th</sup> FISC), April 2–6 2006, Reno, Nevada, USA, 8 pp., 2006.

**Supprimé:** Gaeuman, D., and Rennie, C. D.: A comparison of two field studies of acoustic bed velocity: Grain size and instrument frequency effects, in: Proceedings of the Eighth Federal Interagency Sedimentation Conference (8<sup>th</sup> FISC), April 2–6 2006, Reno, Nevada, USA, 8 pp., 2006.¶



1159 Kondolf, G. M., Schmitt, R. J. P., Carling, P., et al.: Changing sediment budget of the Mekong: Cumulative threats  
1160 and management strategies for a large river basin. *Sci Total Environ.*, 625, 114-134,  
1161 <https://doi.org/10.1016/j.scitotenv.2017.11.361>, 2018.

1162 Kostaschuk, R., and Villard, P.: Flow and sediment transport over large subaqueous dunes: Fraser River, Canada,  
1163 *Sedimentology*, 43 (5), 849-863, <https://doi.org/10.1111/j.1365-3091.1996.tb01506.x>, 1996.

1164 Kostaschuk, R., Best, J., Villard, P., Peakall, J., and Franklin, M.: Measuring flow velocity and sediment transport  
1165 with an acoustic Doppler current profiler, *Geomorphology*, 68, 25-37,  
1166 <https://doi.org/10.1016/j.geomorph.2004.07.012>, 2005.

1167 Latosinski, F. G., Szupiany, R. N., Guerrero, M., Amsler, M. L., and Vionnet, C.: The ADCP's bottom track capability  
1168 for bedload prediction: Evidence on method reliability from sandy river applications, *Flow Measurement and*  
1169 *Instrumentation*, 54, 124-135, <https://doi.org/10.1016/j.flowmeasinst.2017.01.005>, 2017.

1170 Leary, K. C. P., and Buscombe, D.: Estimating sand bed load in rivers by tracking dunes: a comparison of methods  
1171 based on bed elevation time series, *Earth Surf. Dynam.*, 8, 161-172, <https://doi.org/10.5194/esurf-8-161-2020>,  
1172 2020.

1173 Le Guern, J., Rodrigues, S., Tassi, P., Jugé, P., Handfus, T., Duperray, A., and Berrault, P.: Influence of migrating  
1174 bars on dune geometry, in: *Book of Abstracts of the 6th Marine and River Dune Dynamics conference*, 1-3 April  
1175 2019, Bremen, Germany, 157-160, 2019a.

1176 Le Guern, J., Rodrigues, S., Tassi, P., Jugé, P., Handfus, T., and Duperray, A.: Initiation, growth and interactions  
1177 of bars in a sandy-gravel bed river, in: *Book of Abstracts of the 11th Symposium on River, Coastal and Estuarine*  
1178 *Morphodynamics*, 16-21 November 2019, Auckland, New-Zealand, 226 pp., 2019b.

1179 Marineau, M. D., Wright, S. A., and Gaeuman, D.: Calibration of sediment-generated noise measured using  
1180 hydrophones to bedload transport in the Trinity River, California, USA, in: *Proceeding of River Flow 2016 - eighth*  
1181 *International Conference on Fluvial Hydraulics*, Saint Louis, USA, 12-15 July 2016, 1519–1526, 2016.

1182 Mendoza, A., Abad, J. D., Langendoen, E. J., Wang, D., Tassi, P., and El Kadi Abderrezzak, K.: Effect of Sediment  
1183 Transport Boundary conditions on the Numerical Modeling of Bed Morphodynamics, *J. Hydraul. Eng.*, 143 (4),  
1184 [https://doi.org/10.1061/\(ASCE\)HY.1943-7900.0001208](https://doi.org/10.1061/(ASCE)HY.1943-7900.0001208), 2017.

1185 Nittrouer, J. A., Allison, M. A., and Campanella, R.: Bedform transport rates for the lowermost Mississippi River, *J.*  
1186 *Geophys. Res.*, 113, F03004, <https://doi.org/10.1029/2007JF000795>, 2008.

1187 Peters, J. J.: Discharge and Sand Transport in the Braided Zone of the Zaire Estuary, *Netherlands Journal of Sea*  
1188 *Research*, 12, 273-292, [https://doi.org/10.1016/0077-7579\(78\)90031-5](https://doi.org/10.1016/0077-7579(78)90031-5), 1978.

1189 Ramooz, R., and Rennie, C. D.: Laboratory Measurement of Bedload with an ADCP, U.S. Geological Survey  
1190 Scientific Investigations Report, 2010-5091, 2010.

1191 Reesink, A. J. H., Parsons, D. R., and Thomas, R. E.: Sediment transport and bedform development in the lee of  
1192 bars: Evidence from fixed- and partially-fixed bed experiments, in: Proceeding of River Flow 2014 - seventh  
1193 International Conference on Fluvial Hydraulics, Lausanne, Switzerland, 3-5 Septembre 2014, 8 pp., 2014,  
1194 Rennie, C. D., and Millar, R. G.: Measurement of the spatial distribution of fluvial bedload transport velocity in both  
1195 sand and gravel, *Earth Surf. Process. Landforms*, 29, 1173-1193, doi:10.1002/esp.1074, 2004.  
1196 Rennie, C. D., and Villard, P. V.: Site specificity of bed load measurement using an acoustic Doppler current profiler,  
1197 *J. Geophys. Res.*, 109, F03003, <https://doi.org/10.1029/2003JF000106>, 2004.  
1198 Rennie, C. D., Millar, R. G., and Church, M. A.: Measurement of Bed Load Velocity using an Acoustic Doppler  
1199 Current Profiler, *J. Hydraul. Eng.*, 128 (5), 473-483, [https://doi.org/10.1061/\(ASCE\)0733-9429\(2002\)128:5\(473\)](https://doi.org/10.1061/(ASCE)0733-9429(2002)128:5(473)),  
1200 2002.  
1201 Rennie, C. D., Vericat, D., Williams, R. D., Brasington, J., and Hicks, M.: Calibration of acoustic doppler current  
1202 profiler apparent bedload velocity to bedload transport rate, in: *Gravel-Bed Rivers: Processes and Disasters*,  
1203 Oxford, UK: Wiley Blackwell, 209–233, <https://doi.org/10.1002/9781118971437.ch8>, 2017.  
1204 Rodrigues, S., Mosselman, E., Claude, N., Wintenberger, C. L., and Jugé, P.: Alternate bars in a sandy gravel bed  
1205 river: generation, migration and interactions with superimposed dunes, *Earth Surf. Process. Landforms*, 40 (5),  
1206 610-628, <https://doi.org/10.1002/esp.3657>, 2015.  
1207 Simons, D. B., Richardson, E. V., and Nordin, C. F. Jr.: Bedload Equation for Ripples and Dunes, U.S. Geol. Survey  
1208 Prof. Paper, 462-H, <https://doi.org/10.3133/pp462H>, 1965.  
1209 Syvitski, J. P. M., and Milliman, J. D.: Geology, Geography, and Humans Battle for Dominance over the Delivery of  
1210 Fluvial Sediment to the Coastal Ocean, *The Journal of Geology*, 15(1), 1-19, <https://doi.org/10.1086/509246>, 2007.  
1211 Ten Brinke, W. B. M., Wilbers, A. W. E., and Wesseling, C.: Dune growth, decay and migration rates during a large-  
1212 magnitude flood at a sand and mixed sand-gravel bed in the Dutch Rhine river system, in: *In Fluvial Sedimentology*  
1213 VI, Vol. 28 of Special Publications of the International Association of Sedimentologists, 15-32,  
1214 <https://doi.org/10.1002/9781444304213.ch2>, 1999.  
1215 Thorne, P. D., Heathershaw, A. D., and Troiano, L.: Acoustic Detection of Seabed Gravel Movement in Turbulent  
1216 Tidal Currents, *Marine Geology*, 54, M43-M48, [https://doi.org/10.1016/0025-3227\(84\)90035-5](https://doi.org/10.1016/0025-3227(84)90035-5), 1984.  
1217 Thorne, P. D.: The measurement of acoustic noise generated by moving artificial sediments, *J. Acoust. Soc. Am.*,  
1218 78 (3), 1013–1023, <https://doi.org/10.1121/1.393018>, 1985.  
1219 Thorne, P. D.: Laboratory and marine measurements on the acoustic detection of sediment transport, *J. Acoust.*  
1220 *Soc. Am.*, 80(3), 899, <https://doi.org/10.1121/1.393913>, 1986.  
1221 Thorne, P. D.: An overview of underwater sound generated by interparticle collisions and its application to the  
1222 measurements of coarse sediment bedload transport, *Earth Surf. Dyn.*, 2 (2), 531–543,  
1223 <https://doi.org/10.5194/esurf-2-531-2014>, 2014.

Supprimé: 2016

Supprimé: 2016

Supprimé: Rodrigues, S., Claude, N., Jugé, P., and Bréhéret, J. G.: An opportunity to connect the morphodynamics of alternate bars with their sedimentary products, *Earth Surf. Process. Landforms*, 37, 240-248, <https://doi.org/10.1002/esp.2255>, 2012.¶

1231 Van den Berg, J. H.: Bedform migration and bed-load transport in some rivers and tidal environments,  
1232 Sedimentology, 34, 681-698, <https://doi.org/10.1111/j.1365-3091.1987.tb00794.x>, 1987.

1233 Van der Mark, C. F., and Blom, A.: A new and widely applicable tool for determining the geometric properties of  
1234 bedforms, Civil Engineering & Management Research Report 2007R-003/WEM-002 ISSN 1568-4652, University  
1235 of Twente, Enschede, Netherlands, 57 pp., 2007.

1236 Van Rijn, L. C.: Sediment Transport. Part I: Bed Load Transport, J. Hydraul. Eng., 110, 1431-1456,  
1237 [https://doi.org/10.1061/\(ASCE\)0733-9429\(1984\)110:10\(1431\)](https://doi.org/10.1061/(ASCE)0733-9429(1984)110:10(1431)), 1984.

1238 [Van Rijn, L. C., and Gaweesh, M. T. K.: New Total Sediment-Load Sampler, J. Hydraul. Eng., 118 \(12\), 1686–  
1239 1691. https://10.1061/\(ASCE\)0733-9429\(1992\)118:12\(1686\), 1992.](https://doi.org/10.1061/(ASCE)0733-9429(1992)118:12(1686))

1240

1241 Villard, P. V., and Church, M.: Bar and dune development during a freshet: Fraser River Estuary, British Columbia,  
1242 Canada, Sedimentology, 52, 737-756, <https://doi.org/10.1111/j.1365-3091.2005.00721.x>, 2005.

1243 Villard, P., Church, M., and Kostaschuk, R.: Estimating bedload in sand-bed channels using bottom tracking from  
1244 an acoustic Doppler profiler, Spec. Publs int. Ass. Sediment, 35, 197-209,  
1245 <https://doi.org/10.1002/9781444304350.ch12>, 2005.

1246 Vörösmarty, C., McIntyre, P., Gessner, M., Dudgeon, D., Prusevich, A., Green, P., Glidden, S., Bunn, S. E.,  
1247 Sullivan, C. A., Reidy Liermann, C., and Davies, P. M.: Global threats to human water security and river biodiversity,  
1248 Nature, 467, 555–561, <https://doi.org/10.1038/nature09440>, 2010.

1249 Wilbers, A.: The development and hydraulic roughness of subaqueous dunes, Neth. Geogr. Stud, Fac. of Geosci.,  
1250 Utrecht Univ., Utrecht, Netherlands. 323, 224 pp., 2004.

1251 Williams, R. D., Rennie, C. D., Brasington, J., Hicks, D. M., and Vericat, D.: Linking the spatial distribution of bed  
1252 load transport to morphological change during high-flow events in shallow braided river, J. Geophys. Res. Earth  
1253 Surf., 120, 604–622, <https://doi.org/10.1002/2014JF003346>, 2015.